



HAL
open science

A variational-based homogenization model for plastic shakedown analysis of porous materials with a large range of porosity

J Zhang, J. Shao, Q Z Zhu, Géry de Saxce

► **To cite this version:**

J Zhang, J. Shao, Q Z Zhu, Géry de Saxce. A variational-based homogenization model for plastic shakedown analysis of porous materials with a large range of porosity. *International Journal of Mechanical Sciences*, 2021, 199, 10.1016/j.ijmecsci.2021.106429 . hal-04508740

HAL Id: hal-04508740

<https://hal.science/hal-04508740v1>

Submitted on 22 Jul 2024

HAL is a multi-disciplinary open access archive for the deposit and dissemination of scientific research documents, whether they are published or not. The documents may come from teaching and research institutions in France or abroad, or from public or private research centers.

L'archive ouverte pluridisciplinaire **HAL**, est destinée au dépôt et à la diffusion de documents scientifiques de niveau recherche, publiés ou non, émanant des établissements d'enseignement et de recherche français ou étrangers, des laboratoires publics ou privés.



Distributed under a Creative Commons Attribution - NonCommercial 4.0 International License

A variational-based homogenization model for plastic shakedown analysis of porous materials with a large range of porosity

J. Zhang^a, J.F. Shao^{a,b,*}, Q.Z. Zhu^a, G. De Saxcé^b

^aKey Laboratory of Ministry of Education for Geomechanics and Embankment Engineering, Hohai University, Nanjing, China

^bUniv. Lille, CNRS, Centrale Lille, UMR 9013 - LaMcube - Laboratoire de mécanique multiphysique et multiéchelle, Lille, F-59000, France

Abstract

In this paper, a new homogenization model is developed for the determination of macroscopic shakedown limit state for porous media subjected to general cyclic loads. Based on the variational principle over the stabilized cycle, a new macroscopic fatigue criterion is established, beyond which the collapse of material will occur due to fatigue. Unlike the classical Melan's theory by statical approaches relying on the complex construction of a time-independent residual stress field, the formulation of the new criterion is derived from a variational-based kinematical approach which allows overcoming this difficulty. Dirac's measure is adopted to simplify the volume integral with the assumption of vanishing plastic strain increment over a stabilized cycle. The established criteria exhibit directly the dependence of the plastic shakedown limit load on the invariants of the macroscopic stress tensor, Poisson's ratio of the solid matrix and the porosity. The macroscopic safety domain is defined by the intersection of limit surface of this new fatigue criteria and that corresponds to the incremental collapse which is reached monotonically. The theoretical predictions of shakedown limits by the new criterion are compared with the numerical results obtained from non-linear optimization method and with those given by some representative existing criteria. It is shown that the new criterion significantly improves the accuracy of plastic shakedown limit prediction for porous materials with large values of porosity.

Keywords: Porous materials, Cyclic loading, Fatigue, Strength criteria, Variational principle, Homogenization

*Corresponding author.

Email address: jian-fu.shao@polytech-lille.fr (J.F. Shao)

1. Introduction

30 Many engineering materials contain voids or pores at different scales. The macroscopic mechanical behaviour and failure process of porous materials are generally characterized by plastic deformation and void growth. Moreover, in many engineering applications, those materials are subjected to variable or cyclic mechanical loads. It is primordial to predict the material strength under cyclic loading for the durability analysis of engineering structures.

35 During several decades, a large number of studies have been devoted to the determination of macroscopic plastic yield or strength criteria explicitly including effects of voids and their evolutions. Different homogenization methods have been developed, mainly based on limit analysis theory and variational principles. Using a kinematical approach in the framework of limit analysis, the pioneer's work was done by Gurson [25] by formulating the
40 macroscopic strength criterion of porous media with a von Mises type solid matrix. Based on this work, numerous extensions have been proposed in the literature by introducing several modifications. For instance, the well-known numerically motivated GTN model, developed by Tvergaard [59, 60] incorporating three additional parameters, is widely used in structural computations, considering that Gurson's model appears too stiff. Among the other exten-
45 sions of Gurson's model, important efforts have been focused on the consideration of void shape effects [21, 22, 37, 44, 45]. Benzerga and Besson [3] firstly considered the matrix plastic anisotropy of ductile porous media containing spherical pores, which was later extended to spheroidal ones in [43, 32] and to tension-compression asymmetry in [8]. More narrowly, the plastic compressibility of the matrix was considered by adopting pressure-sensitive solid
50 matrix, for instance, a Mises-Schleicher, a Drucker-Prager or a Mohr-Coulomb type matrix for geomaterials [1, 24, 31, 46]. For completeness, some other applications have also been devoted to rigid inclusions-reinforced porous materials [18, 52]. These kinematical approaches provide an upper bound of macroscopic strength surface of porous materials, requiring the choice of a suitable trial velocity field. On the other hand, by using a dual statical ap-
55 proach originally developed from Green's work [23], lower bounds of macroscopic strength criterion have been established in [56, 57]. Recently, an innovative stress-based variational model (SVM) has been developed by [9, 53]. The SVM model combines the Hill variational principle for rigid plastic solids and homogenization concept to deliver macroscopic strength criteria of porous materials.

60 However, most of those criteria are devoted to the prediction of yield stress or failure strength of porous materials under monotonic loading or during the first loading cycle. According to wide experiment data [33, 73, 70], the ultimate limit load under cyclic loading can be very different with that estimated for monotonic case. Generally, three different asymptotic responses can be distinguished under cyclic loads. The first one is the incremental
65 collapse or failure due to excessive accumulated plastic deformation. The second state is related to fatigue induced by alternative plastic deformation of equal amplitude but opposite sign [39, 27, 64] during cycles. The third one is the shakedown state at which the mechanical response becomes purely elastic after a transient phase [49, 16].

The direct way to determine the limit state under cyclic loading is to perform laborious
70 step-by-step computation over all cycles. In order to avoid this, the shakedown theory has

been developed to provide directly some essential information of limit state. The shakedown theory has firstly been based on the extension of limit analysis initially used for monotonic loading and a detailed review can be found in [38, 63]. Similar to limit analysis, both the statical and kinematical approaches are studied for cyclic loads. The statical approach, initiated by Melan [42] and further developed in [58, 35], gives a sufficient context for the evolution to shakedown state of perfect elasto-plastic bodies. The key step of that approach is to find out a time-independent residual stress field. This is usually a difficult task. The kinematical approach, initially proposed by Koiter [34] and completed by [20, 50], is based on an admissible plastic strain increment field. **In general, the real shakedown limit load is restrained by the respective approximate application of the statical and kinematical approaches through relaxing the admissible conditions.** Besides, during the last decades, different numerical methods have been developed concerning hardening effects of materials [30, 29], multi-dimension and multi-field condition [47, 19, 61], multi-layered structure [72, 48], structure's imperfection [71, 2], and eventually porous media considering the void influence [41, 36, 65], with the computational capacity improvement of computers.

On the other hand, important efforts have also been made to extend the basic variational principles initiated by Hill [28] and Markov [40] for monotonic loading to shakedown analysis under cyclic loading. In particular, **Save et al. [49] proposed** two dual methods by using the admissible time-independent residual stress field and plastic strain increment in the sense of Melan and Koiter to develop variational approaches. Especially by considering that the plastic strain over a stabilized cycle vanishes, an upper bound approach for the shakedown analysis was deduced from Markov principle. This approach is consistent with the micro-macro approach developed for high-cycle multi-axial fatigue analysis [13, 14]. It is concluded that the fatigue criterion can be obtained by maximizing the size of strength domain until the limit state for **plastic shakedown** is reached [15].

Concerning the application of Melan's statical theorem to the conservative predictions of macroscopic **plastic shakedown limit loads**, significant advances have been obtained for porous media with perfectly plastic matrix obeying von Mises [68, 67] and Drucker-Prager [66] yield laws, coupled with homogenization theory. Moreover, the kinematical hardening solid phase has been recently studied in [69] with the same methodology by considering Feng's corollary [17] of standard lower shakedown theorem. **The plastic shakedown limit** of porous media considering kinematical hardening effects is proved identical to the perfectly plastic one by both analytical and numerical results. Although the obtained shakedown criteria in this series of works provide a comparatively direct way to evaluate the bearing capacity of porous media, two remarks of such methodology must be pointed out: i) The construction of time-independent residual stress field is quite complex and leads to heavy expressions with numerous terms, in order to meet the requirement of being statically admissible. This is the most important concept of Melan's theorem. Even if it can be eliminated in the final expression by a small trick in [69], it still need to be considered during the derivation. ii) Important differences are still observed between the theoretical predictions and numerical results for large values of porosity ($f > 0.1$), which requires a refinement of the adopted stress fields.

Therefore, the main objective of the present study is to develop a new homogenization

method for determining macroscopic fatigue criteria of porous materials with a large range
 115 of porosity, without considering the time-independent residual stress field. Unlike the above
 mentioned works based on Melan's statical theorem, despite also being within the framework
 of micromechanics with a hollow sphere model, this paper is derived from the [kinematical
 solution](#) [49] for the thick wall tube under isotropic pressure, which is initially developed
 with Markov's variational principle over a single cycle. The special technique of bounded
 120 measures is used to simplify the mathematical derivation by eliminating the volume integral.
 In the same spirit of the Gurson-like homogeneous approaches [9, 53], both the stress and
 strain fields are composed of a hydrostatic part and a pure deviatoric one. Concerning the
 second remark in the previous paragraph, a new trial elastic stress field in the fictitious body
 under pure shear loading is constructed semi-analytically in order to improve the accuracy
 125 of the theoretical result, especially for high values of porosity.

The present paper is organized as follows. In Section 2, we briefly recall the homoge-
 nization theory and the variational principle for the shakedown problem. Section 3 is then
 devoted to determination of the macroscopic fatigue criterion under general cyclic loading
 conditions. In Section 4, the assessment of the new fatigue criterion is presented by compar-
 130 ison with numerical results obtained from non-linear optimization and with some analytical
 solutions given in [67]. Some conclusions and prospectives are presented in the last section.
 In addition, the implementation of [the kinematical solution](#) of the thick wall tube under
 isotropic pressure and the construction of the new fictitious elastic stress field are provided
 in the appendix.

135 2. Basic definitions and homogeneous variational formulations for shakedown problem

The porous material is here represented by a reference unit volume Ω composed of a void
 ω and a solid matrix $\Omega_M = \Omega - \omega$ made of elastic perfectly plastic material, obeying the
 local yield criterion:

$$F(\boldsymbol{\sigma}) \leq 0 \quad (1)$$

140 where F is the yield function and $\boldsymbol{\sigma}$ denotes the stress tensor.

The strain rate tensor is given by the normality law:

$$\dot{\boldsymbol{\epsilon}}^p = \dot{\lambda} \frac{\partial F}{\partial \boldsymbol{\sigma}} \quad (2)$$

where $\dot{\lambda} \geq 0$ is a positive scalar multiplier.

The plastic dissipation function is obtained as

$$\mathcal{D}(\dot{\boldsymbol{\epsilon}}^p) = \boldsymbol{\sigma} : \dot{\boldsymbol{\epsilon}}^p \quad (3)$$

if $\dot{\boldsymbol{\epsilon}}^p$ is associated to $\boldsymbol{\sigma}$.

145 According to the average-field theory for homogenization, the macroscopic stress $\boldsymbol{\Sigma}$ is
 classically defined as the volume average of its microscopic counterpart $\boldsymbol{\sigma}$:

$$\boldsymbol{\Sigma} = \langle \boldsymbol{\sigma} \rangle = \frac{1}{|\Omega|} \int_{\Omega} \boldsymbol{\sigma} \, dV \quad (4)$$

The set of statically admissible [stress fields](#) is defined as:

$$\mathcal{S}_a = \{\boldsymbol{\sigma} \text{ s.t. } \operatorname{div} \boldsymbol{\sigma} = \mathbf{0} \text{ in } \Omega, \boldsymbol{\sigma} \cdot \mathbf{n} = \mathbf{0} \text{ on } \partial\omega, \boldsymbol{\sigma} = \mathbf{0} \text{ in } \omega\} \quad (5)$$

in which \mathbf{n} is the unit outward normal vector of the matrix. Similarly, the set of kinematical admissible velocity fields is given by:

$$\mathcal{K}_a = \{\mathbf{v} \text{ s.t. } \mathbf{v}(\mathbf{x}) = \mathbf{D} \cdot \mathbf{x} \text{ on } \partial\Omega\} \quad (6)$$

150 where [D](#) is the macroscopic strain rate tensor and \mathbf{x} is the position vector on the boundary.

The total local stresses in perfectly elasto-plastic body Ω under variable loadings is divided into two parts [63]:

$$\boldsymbol{\sigma} = \boldsymbol{\sigma}^E + \boldsymbol{\rho} \quad (7)$$

where $\boldsymbol{\sigma}^E$ represents the fictitious purely elastic responses subjected to the very same load, and $\boldsymbol{\rho}$ is the corresponding residual stresses belonging to the following set:

$$\mathcal{N} = \{\boldsymbol{\rho} \text{ s.t. } \operatorname{div} \boldsymbol{\rho} = \mathbf{0} \text{ in } \Omega, \boldsymbol{\rho} \cdot \mathbf{n} = \mathbf{0} \text{ on } \partial\omega, \boldsymbol{\rho} = \mathbf{0} \text{ in } \omega\} \quad (8)$$

155 Let $(\boldsymbol{\sigma}^E, \boldsymbol{\varepsilon}^E, \mathbf{u}^E)$ be the fictitious purely elastic responses of the elementary cell Ω under the same loads. Likewise, the field defined by:

$$\boldsymbol{\eta} = \boldsymbol{\varepsilon} - \boldsymbol{\varepsilon}^E \quad (9)$$

belongs to the set of residual strain fields defined by:

$$\mathcal{N}^* = \{\boldsymbol{\eta} \mid \exists \mathbf{v} \text{ s.t. } \boldsymbol{\eta} = \operatorname{grad}_s \mathbf{v}, \mathbf{v} = \mathbf{0} \text{ on } \partial\Omega\} \quad (10)$$

Let us introduce the definition of admissible plastic strain rate field to distinguish the collapse process over a load cycle for a periodic action in Koiter's sense [34]. For a considered
160 plastic strain rate field $\dot{\boldsymbol{\varepsilon}}^p$, such that

- the increment of the plastic strain on the load cycle is kinematically admissible:

$$\Delta \boldsymbol{\varepsilon}^p = \oint \dot{\boldsymbol{\varepsilon}}^p dt \in \mathcal{N}^* \quad (11)$$

with zero values on the boundary.

- $\dot{\boldsymbol{\varepsilon}}^p$ is plastically admissible:

$$\int_{\Omega} \oint \boldsymbol{\sigma}^E : \dot{\boldsymbol{\varepsilon}}^p dt dV > 0 \quad (12)$$

$\dot{\boldsymbol{\varepsilon}}^p$ is said to be an admissible plastic strain rate field.

165 Based on this ground, the kinematical shakedown theorem is proved by Halphen [26]: *If an admissible plastic strain rate field can be found, the structure does not shake down.*

For the structure in shakedown state, the applied external actions can be replaced by the corresponding stress field $\boldsymbol{\sigma}^E$ in the fictitious elastic body. The following variational principle for shakedown problem is developed by Save et al. [49]:

170 **Markov's principle over a cycle**¹: Among the admissible plastic strain rate fields $\dot{\boldsymbol{\epsilon}}^p$, the true one $\dot{\boldsymbol{\epsilon}}^p$ makes the functional:

$$\Phi(\dot{\boldsymbol{\epsilon}}^p) = \int_{\Omega} \oint \mathcal{D}(\dot{\boldsymbol{\epsilon}}^p) dt dV - \int_{\Omega} \oint \boldsymbol{\sigma}^E : \dot{\boldsymbol{\epsilon}}^p dt dV \quad (13)$$

the minimum value.

In particular, for an admissible couple $(\dot{\boldsymbol{\epsilon}}^p, \bar{\boldsymbol{\rho}})$ such that the admissible plastic strain rate field $\dot{\boldsymbol{\epsilon}}^p$ is associated to the stress field $(\boldsymbol{\sigma}^E + \bar{\boldsymbol{\rho}})$ by the normality law with the time-independent residual stress field $\bar{\boldsymbol{\rho}}$, according to (3), one has:

$$\Phi_0(\dot{\boldsymbol{\epsilon}}^p, \boldsymbol{\sigma}^E) = 0 \quad (14)$$

in which Φ_0 denotes the minimum value of the functional Φ introduced in (13).

Further, by considering the principle of virtual work, one gets:

$$\int_{\Omega} \oint \bar{\boldsymbol{\rho}} : \dot{\boldsymbol{\epsilon}}^p dt dV = \int_{\Omega} \bar{\boldsymbol{\rho}} : \Delta \boldsymbol{\epsilon}^p dV = 0 \quad (15)$$

Indeed, it is difficult to find a general solution for the admissible couple $(\dot{\boldsymbol{\epsilon}}^p, \bar{\boldsymbol{\rho}})$, because the fictitious elastic stress field $\boldsymbol{\sigma}^E$ also contributes to the associated total stress field. As proved by [4], it is convenient to determine the true elastic stress field $\boldsymbol{\sigma}^E$ and then find the best admissible strain rate field by solving the following minimization problem:

$$\Phi_0(\dot{\boldsymbol{\epsilon}}^p, \boldsymbol{\sigma}^E) = \min_{\dot{\boldsymbol{\epsilon}}^p \in \mathcal{N}^*} \Phi_0(\dot{\boldsymbol{\epsilon}}^p, \boldsymbol{\sigma}^E) = 0 \quad (16)$$

Replacing the local elastic stress field by the invariants of the macroscopic stress tensor, a homogeneous criterion of porous media for the shakedown problem is finally written as:

$$\mathcal{F}(\boldsymbol{\Sigma}) = \int_{\Omega} \oint \mathcal{D}(\dot{\boldsymbol{\epsilon}}^p) dt dV - \int_{\Omega} \oint \boldsymbol{\sigma}^E(\boldsymbol{\Sigma}) : \dot{\boldsymbol{\epsilon}}^p dt dV = 0 \quad (17)$$

Obviously, the next step is the choice of a trial stress field depending on some parameters, rich enough to capture the main physical characteristics. It must be remarked that, in order to simplify the calculation, the minimum of Φ_0 may not strictly be equal to zero but satisfying the admissible condition only in an average sense for the trial fields. Nevertheless, according to previous studies [9, 11], this minimum principle still provides a best solution within the framework imposed by the approximations. Different from the previous studies devoted to transforming the yield criterion at micro scale to the macroscopic one, the above homogeneous shakedown formulation (17) is on account of the equivalence between the plastic dissipation and the external work rate in nature.

¹It is an extension of the variational principle in Limit Analysis to shakedown problem by considering the critical load cycle, which is firstly introduced by Markov for perfectly plastic material. The reader is referred to [62] for the rigorous demonstration.

3. Construction of the stress and strain rate fields and determination of macroscopic fatigue criterion under general cyclic loadings

195 A hollow sphere model is adopted as the [representative volume element \(RVE\)](#) of porous media. The inner and outer radius are noted as a and b respectively, giving the void volume fraction $f = (a/b)^3 < 1$. The solid matrix is supposed to be made of elastic perfectly plastic material obeying von Mises yield criterion:

$$F(\boldsymbol{\sigma}) = \sigma_{eq}(\boldsymbol{\sigma}) - \sigma_y \leq 0 \quad (18)$$

where $\sigma_{eq}(\boldsymbol{\sigma}) = \sqrt{\frac{3}{2} \mathbf{s} : \mathbf{s}}$ denotes the equivalent stress with \mathbf{s} being the deviatoric part
 200 $\mathbf{s} = \boldsymbol{\sigma} - tr(\boldsymbol{\sigma})\mathbf{1}$.

The cyclic loadings are enforced proportional at the macro scale during each cycle with a constant stress triaxiality:

$$T = \Sigma_m / \Sigma_{eq} \quad (19)$$

where Σ_m and Σ_{eq} are the macroscopic mean stress and equivalent stress.

For the pure hydrostatic loading case ($\Sigma_{eq} = 0$), [Save et al. \[49\]](#) proposed an exact
 205 [solution](#) initially for the thick wall tube under isotropic loadings using Markov's principle over a cycle. The implementation on the hollow sphere model is outlined in [Appendix A](#). While for the general cyclic loading case, the trial microscopic elastic stress and plastic strain rate fields are firstly constructed in the following subsection. Then a macroscopic fatigue criterion is established for porous media by the use of the homogeneous formulation (17).

3.1. Trial elastic stress and plastic strain rate fields combined between hydrostatic and deviatoric loadings

In order to limit the errors due to approximations, we shall consider trial fields for which the macroscopic model is exact at least for pure hydrostatic loadings provided in the previous section. And taking account of the symmetric hollow sphere model, both the trial
 215 stress fields and plastic strain rate fields are considered as the sum of two decompositions in spherical and deviatoric parts:

- 1) For the fictitious elastic stress field, a heterogeneous part $\boldsymbol{\sigma}^{E(1)}$ corresponding to the exact one generated by the pure hydrostatic loading is taking the same form of (61):

$$\boldsymbol{\sigma}^{E(1)} = \frac{\Sigma_m}{1-f} \left(\mathbf{1} + \frac{1}{2} \left(\frac{a}{r} \right)^3 (\mathbf{e}_\theta \otimes \mathbf{e}_\theta + \mathbf{e}_\phi \otimes \mathbf{e}_\phi - 2 \mathbf{e}_r \otimes \mathbf{e}_r) \right) \quad (20)$$

The second part $\boldsymbol{\sigma}^{E(2)}$ is added to capture the shear effects in the fictitious body. Based
 220 on Papkovitch-Neuber solution [55] of a hollow sphere under pure deviatoric tractions on its outer boundary, a trial elastic stress field writes in the following form in the

spherical frame $\{\mathbf{e}_r, \mathbf{e}_\theta, \mathbf{e}_\phi\}$:

$$\begin{aligned}
\boldsymbol{\sigma}^{E(2)} = & 2M_0 \left\{ \left[\left(-6\nu A_2 r^2 + 2B_2 - \frac{2(10-2\nu)C_2}{r^3} + \frac{12D_2}{r^5} \right) \left(\frac{3\cos^2\theta - 1}{2} \right) \right] (\mathbf{e}_r \otimes \mathbf{e}_r) \right. \\
& + \left[\left(-3(2\nu + 14)A_2 r^2 - 4B_2 + \frac{2(2\nu - 1)C_2}{r^3} - \frac{9D_2}{r^5} \right) \left(\frac{3\cos^2\theta - 1}{2} \right) \right. \\
& + \left. \left((7 - 4\nu)A_2 r^2 + B_2 + \frac{(2 - 4\nu)C_2}{r^3} + \frac{D_2}{r^5} \right) (3\cos^2\theta) \right] (\mathbf{e}_\theta \otimes \mathbf{e}_\theta) \\
& + \left[\left(-30\nu A_2 r^2 + 2B_2 + \frac{2(5 - 10\nu)C_2}{r^3} - \frac{3D_2}{r^5} \right) \left(\frac{3\cos^2\theta - 1}{2} \right) \right. \\
& - \left. \left((7 - 4\nu)A_2 r^2 + B_2 + \frac{(2 - 4\nu)C_2}{r^3} + \frac{D_2}{r^5} \right) (3\cos^2\theta) \right] (\mathbf{e}_\phi \otimes \mathbf{e}_\phi) \\
& \left. - \left[\left((2\nu + 7)A_2 r^2 + B_2 + \frac{(2 + 2\nu)C_2}{r^3} - \frac{4D_2}{r^5} \right) (3\cos\theta \sin\theta) \right] (\mathbf{e}_r \otimes \mathbf{e}_\theta + \mathbf{e}_\theta \otimes \mathbf{e}_r) \right\} \quad (21)
\end{aligned}$$

where M_0 is a constant and ν denotes Poisson's ratio. The detailed determination of $\boldsymbol{\sigma}^{E(2)}$ and the expression of A_2, B_2, C_2, D_2 are given in Appendix B.

Moreover, if the residual stress field is statically admissible $\boldsymbol{\rho} \in \mathcal{N}$, the residual stresses should vanish at macro scale:

$$\boldsymbol{\Sigma}^r = \frac{1}{|\Omega|} \int_{\Omega} \boldsymbol{\rho} \, dV = \frac{1}{|\Omega|} \int_{\partial\Omega} (\boldsymbol{\rho} \cdot \mathbf{n}) \otimes \mathbf{x} \, dS = \mathbf{0} \quad (22)$$

So the macroscopic stress reduces to the corresponding value in the fictitious elastic cell:

$$\boldsymbol{\Sigma} = \boldsymbol{\Sigma}^r + \boldsymbol{\Sigma}^E = \boldsymbol{\Sigma}^E \quad (23)$$

Consequently, combining (20) and (21), the axisymmetric macroscopic stress tensor can be calculated by the average defined in (4):

$$\boldsymbol{\Sigma} = \Sigma_m \mathbf{1} + M_0 N (\mathbf{e}_r \otimes \mathbf{e}_r + \mathbf{e}_\theta \otimes \mathbf{e}_\theta - 2\mathbf{e}_\phi \otimes \mathbf{e}_\phi), \quad (24)$$

with

$$N = \frac{42}{5} A_2 (f^{5/3} - 1) + 2B_2 (f - 1) \quad (25)$$

from which one can compute the macroscopic equivalent stress Σ_{eq} and the third invariant of stress deviator J_3 :

$$\Sigma_{eq} = 3N |M_0|, \quad J_3 = -2N^3 M_0^3. \quad (26)$$

Considering that $0 < f < 1$ and $0 < \nu < 0.5$ and the expressions of A_2 and B_2 given by Eq.(91), one can eventually have $N > 0$.

Then the following relation can be obtained:

$$M_0 = -\text{sign}(J_3) \frac{\Sigma_{eq}}{3N} \quad (27)$$

As a result, replacing M_0 by (27), one obtains the new trial elastic stress field in the fictitious material:

$$\boldsymbol{\sigma}^E = \boldsymbol{\sigma}^{E(1)} + \boldsymbol{\sigma}^{E(2)} \quad (28)$$

2) Next, we adopt the trial velocity field in the following form:

$$\mathbf{v} = \frac{G_1}{r^3} \mathbf{e}_r + 6G_2 (\rho \mathbf{e}_\rho - 2z \mathbf{e}_z) \quad (29)$$

240 where the first term in spherical coordinates is the exact solution for hollow sphere under isotropic loading and the additional two linear terms in cylindrical coordinate systems are inspired from [24] to capture shear effects, leading to an axisymmetric macroscopic strain rate. ρ and z are variables in cylindrical coordinate systems with $r = \sqrt{\rho^2 + z^2}$.

245 However, in order to eliminate the parameters, we propose to derive the plastic strain rate field from the total stress field by using the normality law (2). Considering one singer loading process, the loading condition is the same as the monotonic proportional one if the stress triaxiality remains constant. So that we can adopt the trial stress field established in the limit analysis-based work [9] as the total stress field defined in Eq.(7),

250 in order to produce the plastic strain rate. Consequently, the total stress field beyond the elastic limit with von Mises model inspired from [9] reads:

$$\boldsymbol{\sigma} = \boldsymbol{\sigma}^{(1)} + \boldsymbol{\sigma}^{(2)} \quad (30)$$

$\boldsymbol{\sigma}^{(1)}$ is the exact hydrostatic part in the spherical coordinate:

$$\boldsymbol{\sigma}^{(1)} = -M_1 \left(\ln \left(\frac{a}{r} \right) \mathbf{1} - \frac{1}{2} (\mathbf{e}_\theta \otimes \mathbf{e}_\theta + \mathbf{e}_\phi \otimes \mathbf{e}_\phi) \right) \quad (31)$$

with M_1 being the proportional parameter.

255 $\boldsymbol{\sigma}^{(2)}$ is a homogeneous deviatoric stress field under axisymmetric conditions in the cylindrical coordinates $\{\mathbf{e}_\rho, \mathbf{e}_\phi, \mathbf{e}_z\}$:

$$\boldsymbol{\sigma}^{(2)} = M_2 (\mathbf{e}_\rho \otimes \mathbf{e}_\rho + \mathbf{e}_\phi \otimes \mathbf{e}_\phi - 2\mathbf{e}_z \otimes \mathbf{e}_z) \quad (32)$$

where M_2 is also a constant parameter. Noticing that the equilibrium condition on the void boundary for $\boldsymbol{\sigma}^{(2)}$ is relaxed to the average value:

$$\Sigma_m^{void} = \frac{1}{3|\Omega|} \int_{\Omega} tr(\boldsymbol{\sigma}^{(2)}) dV = \frac{1}{3|\Omega|} \int_{\partial\Omega} (\boldsymbol{\sigma}^{(2)} \cdot \mathbf{n}) \otimes \mathbf{x} dS = 0 \quad (33)$$

260 Considering the normality law (2), one can derive the plastic strain rate field from Eq.(30):

$$\begin{aligned} \dot{\boldsymbol{\epsilon}}^p = & \frac{\dot{\lambda}}{2\sqrt{M_1^2 + 3M_1M_2(1 + 3\cos 2\theta) + 36M_2^2}} [-(2M_1 + 3M_2(1 + 3\cos 2\theta)) \mathbf{e}_r \otimes \mathbf{e}_r \\ & + (M_1 + 3M_2(3\cos 2\theta - 1)) \mathbf{e}_\theta \otimes \mathbf{e}_\theta + (M_1 + 6M_2) \mathbf{e}_\phi \otimes \mathbf{e}_\phi \\ & + 9M_2 \sin 2\theta (\mathbf{e}_r \otimes \mathbf{e}_\theta + \mathbf{e}_\theta \otimes \mathbf{e}_r)] \end{aligned} \quad (34)$$

The equivalent strain rate is calculated for the general loading case:

$$\varepsilon_{eq}(\dot{\boldsymbol{\varepsilon}}^p) = \sqrt{\frac{2}{3} \dot{\boldsymbol{\varepsilon}}^p : \dot{\boldsymbol{\varepsilon}}^p} = \dot{\lambda} \quad (35)$$

where the deviatoric part of the plastic strain rate $\dot{\boldsymbol{\varepsilon}}^p = \dot{\boldsymbol{\varepsilon}}^p - \frac{1}{3} \text{tr}(\dot{\boldsymbol{\varepsilon}}^p) \mathbf{1}$. Noticing that the plastic strain rate field (34) obtained from the total stress field provides the same form with the one derived from the velocity field (29) (see Appendix C for details).

265 3.2. Determination of the macroscopic fatigue criterion

Using Eq.(35), the plastic dissipation in general loading conditions can be calculated as:

$$\mathcal{D}(\dot{\boldsymbol{\varepsilon}}^p) = \sigma_y \varepsilon_{eq}(\dot{\boldsymbol{\varepsilon}}^p) = \sigma_y \dot{\lambda} \quad (36)$$

Besides, resulting from (28) and (34), the local work rate by the external actions reads:

$$\boldsymbol{\sigma}^E : \dot{\boldsymbol{\varepsilon}}^p = - \frac{3\dot{\lambda} \left[-a^3 r^2 M_1 \frac{\Sigma_m}{1-f} - \frac{3a^3 r^2 (1+3 \cos 2\theta)}{2} M_2 \frac{\Sigma_m}{1-f} + P_1 M_1 M_0 + P_2 M_2 M_0 \right]}{2r^5 \sqrt{M_1^2 + 3M_1 M_2 (1 + 3 \cos 2\theta) + 36M_2^2}} \quad (37)$$

with

$$\begin{aligned} P_1 &= (1 + 3 \cos 2\theta) [(7 + 4\nu) r^7 A_2 + r^5 B_2 + (-8 + 12\nu) r^2 C_2 + 6D_2] \\ P_2 &= 24((1 + 3 \cos 2\theta)\nu + 7) r^7 A_2 + 24r^5 B_2 + (24(1 + 3 \cos 2\theta)\nu - 15(1 + 3 \cos 2\theta)^2 + 48) r^2 C_2 \\ &\quad + \frac{9}{2} (35 \cos^2 2\theta + 10 \cos 2\theta - 13) D_2 \end{aligned} \quad (38)$$

270 The homogeneous formulation over a loading cycle (17) then reads:

$$\int_{\Omega} \oint \sigma_y \dot{\lambda} dt dV - \int_{\Omega} \oint \left(\frac{3\dot{\lambda} \left[\left(M_1 + \frac{3(1+3 \cos 2\theta)}{2} M_2 \right) a^3 r^2 \frac{\Sigma_m}{1-f} + (P_1 M_1 + P_2 M_2) \frac{\text{sign}(J_3) \Sigma_{eq}}{3N} \right]}{2r^5 \sqrt{M_1^2 + 3M_1 M_2 (1 + 3 \cos 2\theta) + 36M_2^2}} \right) dt dV = 0 \quad (39)$$

which provides the macroscopic shakedown condition for porous materials. It is remarkable to observe that the above expression in the spherical coordinates not only depends on r , but also is a function of θ , originating from the deviatoric part of the elastic stress field $\boldsymbol{\sigma}^{E(2)}$.

275 As it is shown in [49], the loading cycle integrals can be replaced by average values if we consider the final stabilized state. Likewise the pure hydrostatic loading case in Appendix A, we consider that the components of the plastic strain rate tensor $\dot{\varepsilon}_{ij+}^p$ (resp. $\dot{\varepsilon}_{ij-}^p$) in a stabilized cycle during a unit time interval remain constant, when the macroscopic stress invariants reach simultaneously their extreme values Σ_{m+} and Σ_{eq+} (resp. Σ_{m-} and Σ_{eq-}). Thus, if the collapse occurs by alternating plasticity (fatigue), the increment of the plastic strain over this cycle reads:

$$\oint \dot{\varepsilon}_{ij}^p dt = \Delta \varepsilon_{ij}^p = \dot{\varepsilon}_{ij+}^p + \dot{\varepsilon}_{ij-}^p = 0 \quad (40)$$

in which the corresponding multiplier is noted as $\dot{\lambda}_+$ and $\dot{\lambda}_-$, respectively. Eq.(35) and (40) lead to the following relation:

$$\dot{\lambda}_+ = \dot{\lambda}_- \geq 0 \quad (41)$$

The shakedown limit is reached when the extreme values of cyclic loadings are taken. Considering (40) and (41), the macroscopic shakedown condition (39) can be recast into the following form:

$$\begin{aligned} \int_{\Omega} \sigma_y (\dot{\lambda}_+ + \dot{\lambda}_-) dV - \int_{\Omega} \frac{3\dot{\lambda}_+ \left[\left(M_1 + \frac{3(1+3\cos 2\theta)}{2} M_2 \right) a^3 r^2 \frac{\Sigma_{m+}}{1-f} + (P_1 M_1 + P_2 M_2) \frac{\text{sign}(J_{3+}) \Sigma_{eq+}}{3N} \right]}{2r^5 \sqrt{M_1^2 + 3M_1 M_2 (1 + 3\cos 2\theta)} + 36M_2^2} dV \\ + \int_{\Omega} \frac{3\dot{\lambda}_- \left[\left(M_1 + \frac{3(1+3\cos 2\theta)}{2} M_2 \right) a^3 r^2 \frac{\Sigma_{m-}}{1-f} + (P_1 M_1 + P_2 M_2) \frac{\text{sign}(J_{3-}) \Sigma_{eq-}}{3N} \right]}{2r^5 \sqrt{M_1^2 + 3M_1 M_2 (1 + 3\cos 2\theta)} + 36M_2^2} dV = 0 \end{aligned} \quad (42)$$

and reduces to

$$2 \int_{\Omega} \sigma_y \dot{\lambda}_+ dV - \int_{\Omega} \frac{3\dot{\lambda}_+ \left[\left(M_1 + \frac{3(1+3\cos 2\theta)}{2} M_2 \right) a^3 r^2 \frac{\Delta \Sigma_m}{1-f} + (P_1 M_1 + P_2 M_2) \frac{\Delta(\text{sign}(J_3) \Sigma_{eq})}{3N} \right]}{2r^5 \sqrt{M_1^2 + 3M_1 M_2 (1 + 3\cos 2\theta)} + 36M_2^2} dV = 0 \quad (43)$$

where

$$\Delta \Sigma_m = \Sigma_{m+} - \Sigma_{m-}, \quad \Delta(\text{sign}(J_3) \Sigma_{eq}) = \text{sign}(J_{3+}) \Sigma_{eq+} - \text{sign}(J_{3-}) \Sigma_{eq-}$$

As mentioned in the previous section, the admissible plastic strain rate field always converges to Dirac's measure with the assumption of collapse by fatigue (40). Similar to the derivation of isotropic loadings, it is essential to apply Dirac's measure (71) at certain position in the cell at $r = r_0, \theta = \theta_0$ to avoid the volume integral. The macroscopic shakedown condition (43) is recast to

$$2\sigma_y - \frac{3 \left[\left(M_1 + \frac{3(1+3\cos 2\theta)}{2} M_2 \right) a^3 r^2 \frac{\Delta \Sigma_m}{1-f} + (P_1 M_1 + P_2 M_2) \frac{\Delta(\text{sign}(J_3) \Sigma_{eq})}{3N} \right]}{2r^5 \sqrt{M_1^2 + 3M_1 M_2 (1 + 3\cos 2\theta)} + 36M_2^2} = 0 \quad (44)$$

Regarding the macroscopic shakedown condition (44), the next step is to build an additional relation to eliminate the parameters M_1 and M_2 . Recalling the enforced proportional cyclic loadings, the macroscopic stress triaxiality can be also obtained from the adopted total stress field (30):

$$T = \frac{-\frac{M_1 \ln f}{3}}{-\text{sign}(J_3) 3(1-f) M_2} \quad (45)$$

The reader is referred to [9] for details.

Due to the linear cyclic responses when shakedown occurs, it is readily to build the following relation:

$$\frac{\Sigma_{m+}}{\text{sign}(J_{3+}) \Sigma_{eq+}} = \frac{\Delta \Sigma_m}{\Delta(\text{sign}(J_3) \Sigma_{eq})} = \frac{M_1 \ln f}{\text{sign}(J_3) 9(1-f) M_2} \quad (46)$$

The shakedown condition (44) can be considered as a fatigue criterion to prevent the failure due to alternating plasticity when the amplitude of the cyclic loading takes its maximum value:

$$\frac{9 \left[\left(M_1 + \frac{3(1+3 \cos 2\theta)}{2} M_2 \right) a^3 r^2 \frac{\Delta \Sigma_m}{1-f} + (P_1 M_1 + P_2 M_2) \frac{\Delta(\text{sign}(J_3) \Sigma_{eq})}{3N} \right]^2}{16r^{10} (M_1^2 + 3M_1 M_2 (1 + 3 \cos 2\theta) + 36M_2^2)} - \sigma_y^2 = 0 \quad (47)$$

Replacing M_1, M_2 by the macroscopic stress invariants, one has:

$$\frac{9 \left[\left(\frac{9(1-f)\Delta \Sigma_m}{\Delta(\text{sign}(J_3) \Sigma_{eq}) \ln f} + \frac{3(1+3 \cos 2\theta)}{2} \right) a^3 r^2 \frac{\Delta \Sigma_m}{1-f} + \left(P_1 \frac{9(1-f)\Delta \Sigma_m}{\Delta(\text{sign}(J_3) \Sigma_{eq}) \ln f} + P_2 \right) \frac{\Delta(\text{sign}(J_3) \Sigma_{eq})}{3N} \right]^2}{16r^{10} \left(\left(\frac{9(1-f)\Delta \Sigma_m}{\Delta(\text{sign}(J_3) \Sigma_{eq}) \ln f} \right)^2 + 3 \frac{9(1-f)\Delta \Sigma_m}{\Delta(\text{sign}(J_3) \Sigma_{eq}) \ln f} (1 + 3 \cos 2\theta) + 36 \right)} - \sigma_y^2 = 0 \quad (48)$$

It can be seen from the equivalent stress distribution under pure deviatoric loading (Figure 14) that the most heavily loaded point locates on the void surface at equator ($r = a, \theta = \pi/2$). Recalling that the hollow sphere under isotropic loading also yields firstly on the void surface, it is supposed that the first term of the left part in Eq.(48) takes its extreme value at $r = a$. This leads to:

$$\frac{9 \left[\left(\frac{9(1-f)\Delta \Sigma_m}{\Delta(\text{sign}(J_3) \Sigma_{eq}) \ln f} + \frac{3(1+3 \cos 2\theta)}{2} \right) a^5 \frac{\Delta \Sigma_m}{1-f} + \left(P_1(\theta) \frac{9(1-f)\Delta \Sigma_m}{\Delta(\text{sign}(J_3) \Sigma_{eq}) \ln f} + P_2(\theta) \right) \frac{\Delta(\text{sign}(J_3) \Sigma_{eq})}{3N} \right]^2}{16a^{10} \left(\left(\frac{9(1-f)\Delta \Sigma_m}{\Delta(\text{sign}(J_3) \Sigma_{eq}) \ln f} \right)^2 + 3 \frac{9(1-f)\Delta \Sigma_m}{\Delta(\text{sign}(J_3) \Sigma_{eq}) \ln f} (1 + 3 \cos 2\theta) + 36 \right)} - \sigma_y^2 = 0 \quad (49)$$

where

$$\begin{aligned} P_1(\theta) &= (1 + 3 \cos 2\theta) [(7 + 4\nu) a^7 A_2 + a^5 B_2 + (-8 + 4\nu) a^2 C_2 + 6D_2] \\ P_2(\theta) &= 24 ((1 + 3 \cos 2\theta)\nu + 7) a^7 A_2 + 24a^5 B_2 + (24(1 + 3 \cos 2\theta)\nu - 15(1 + 3 \cos 2\theta)^2 + 48) a^2 C_2 \\ &\quad + \frac{1}{2} (315 \cos^2 2\theta + 90 \cos 2\theta - 117) D_2 \end{aligned} \quad (50)$$

which can be rewritten as:

$$\mathcal{F}(\Sigma) = \frac{9 \left[\frac{9}{\ln f} \Delta \Sigma_m^2 + \left(\frac{3(1+3 \cos 2\theta)}{2(1-f)} + \frac{9(1-f)P_1(\theta)}{3a^5 \ln f N} \right) \Delta \Sigma_m \Delta(\text{sign}(J_3) \Sigma_{eq}) + \frac{P_2(\theta)}{3a^5 N} \Delta(\text{sign}(J_3) \Sigma_{eq})^2 \right]^2}{16 \left(\left(\frac{9(1-f)}{\ln f} \Delta \Sigma_m \right)^2 + \frac{27(1-f)(1+3 \cos 2\theta)}{\ln f} \Delta \Sigma_m \Delta(\text{sign}(J_3) \Sigma_{eq}) + 36 \Delta(\text{sign}(J_3) \Sigma_{eq})^2 \right)} - \sigma_y^2 = 0 \quad (51)$$

The established criterion (51) is succinctly expressed by the amplitude of the macroscopic hydrostatic and deviatoric stresses. For the sake of clarity, we will rewrite this formulation by using the maximum value of the cyclic loads. Let us introduce the macroscopic stress ratio:

$$R = \Sigma_{m-} / \Sigma_{m+} \quad (52)$$

where $-1 \leq R < 1$. Taking account of the enforced proportional cyclic loading process (19),
 315 we have

$$\Sigma_{eq-} / \Sigma_{eq+} = |R|, \quad \text{sign}(J_{3+}) / \text{sign}(J_{3-}) = \text{sign}(R) \quad (53)$$

Referring to Fig.14, the shakedown condition can be detailed as follows by respecting the sign of J_{3+} :

1) When $J_{3+} > 0$, then $\Delta(\text{sign}(J_3)\Sigma_{eq}) > 0$, the macroscopic fatigue criterion becomes:

$$\mathcal{F}_{\theta=\pi/2}^{(+)} = (1 - R)^2 \frac{9 \left[\frac{9}{\ln f} \Sigma_{m+}^2 + \left(\frac{-3}{1-f} + \frac{3(1-f)P_1(\pi/2)}{f^{5/3} \ln f N} \right) \Sigma_{m+} \Sigma_{eq+} + \frac{P_2(\pi/2) \Sigma_{eq+}^2}{3f^{5/3} N} \right]^2}{16 \left[\left(\frac{9(1-f)}{\ln f} \Sigma_{m+} \right)^2 + \frac{-54(1-f)}{\ln f} \Sigma_{m+} \Sigma_{eq+} + 36 \Sigma_{eq+}^2 \right]} - \sigma_y^2 = 0 \quad (54)$$

for the triaxiality $T \geq T_0^2$, where the shakedown condition is guaranteed anywhere in
 320 the cell when it is satisfied at $\theta = \frac{\pi}{2}$ with:

$$\begin{aligned} P_1(\pi/2) &= -2 \left[(7 + 4\nu) f^{7/3} A_2 + f^{5/3} B_2 + (-8 + 4\nu) f^{2/3} C_2 + 6D_2 \right] \\ P_2(\pi/2) &= 24(-2\nu + 7) f^{7/3} A_2 + 24f^{5/3} B_2 - 12(4\nu + 1) f^{2/3} C_2 + 54D_2 \end{aligned} \quad (55)$$

Otherwise, for the triaxiality $T \leq T_0$, the shakedown condition

$$\mathcal{F}_{\theta=0}^{(+)} = (1 - R)^2 \frac{9 \left[\frac{9}{\ln f} \Sigma_{m+}^2 + \left(\frac{6}{1-f} + \frac{3(1-f)P_1(0)}{f^{5/3} \ln f N} \right) \Sigma_{m+} \Sigma_{eq+} + \frac{P_2(0) \Sigma_{eq+}^2}{3f^{5/3} N} \right]^2}{16 \left[\left(\frac{9(1-f)}{\ln f} \Sigma_{m+} \right)^2 + \frac{108(1-f)}{\ln f} \Sigma_{m+} \Sigma_{eq+} + 36 \Sigma_{eq+}^2 \right]} - \sigma_y^2 = 0 \quad (56)$$

should be fulfilled at $\theta = 0$ or π with

$$\begin{aligned} P_1(0) &= 4 \left[(7 + 4\nu) f^{7/3} A_2 + f^{5/3} B_2 + (-8 + 4\nu) f^{2/3} C_2 + 6D_2 \right] \\ P_2(0) &= 24 \left[(7 + 4\nu) f^{7/3} A_2 + f^{5/3} B_2 + (-8 + 4\nu) f^{2/3} C_2 + 6D_2 \right] \end{aligned} \quad (57)$$

2) Similarly, when $J_{3+} < 0$, then $\Delta(\text{sign}(J_3)\Sigma_{eq}) < 0$, the macroscopic shakedown criterion:

$$\mathcal{F}_{\theta=0}^{(-)} = (1 - R)^2 \frac{9 \left[\frac{9}{\ln f} \Sigma_{m+}^2 - \left(\frac{6}{1-f} + \frac{3(1-f)P_1(0)}{f^{5/3} \ln f N} \right) \Sigma_{m+} \Sigma_{eq+} + \frac{P_2(0) \Sigma_{eq+}^2}{3f^{5/3} N} \right]^2}{16 \left[\left(\frac{9(1-f)}{\ln f} \Sigma_{m+} \right)^2 - \frac{108(1-f)}{\ln f} \Sigma_{m+} \Sigma_{eq+} + 36 \Sigma_{eq+}^2 \right]} - \sigma_y^2 = 0 \quad (58)$$

325 is fulfilled at $\theta = 0$ or π in order to prevent the fatigue collapse for $T \geq -T_0$.

² T_0 is a particular value of triaxiality, of which the fatigue collapse occurs simultaneously at $\theta = \pi/2$ and 0. It depends on f and ν , and can be obtained by solving the equation $\mathcal{F}_{\theta=\pi/2}^{(+)} = \mathcal{F}_{\theta=0}^{(+)}$.

Or, for $T \leq -T_0$, the shakedown condition is ensured at $\theta = \frac{\pi}{2}$, taking the following form:

$$\mathcal{F}_{\theta=\pi/2}^{(-)} = (1 - R)^2 \frac{9 \left[\frac{9}{\ln f} \Sigma_{m+}^2 - \left(\frac{6}{1-f} + \frac{3(1-f)P_1(\pi/2)}{f^{5/3} \ln f N} \right) \Sigma_{m+} \Sigma_{eq+} + \frac{P_2(\pi/2)}{3f^{5/3} N} \Sigma_{eq+}^2 \right]^2}{16 \left[\left(\frac{9(1-f)}{\ln f} \Sigma_{m+} \right)^2 - \frac{108(1-f)}{\ln f} \Sigma_{m+} \Sigma_{eq+} + 36 \Sigma_{eq+}^2 \right]} - \sigma_y^2 = 0 \quad (59)$$

At this point, Eqs.(54) to (59) represent the main contributions of the present paper, giving macroscopic fatigue criteria for ductile porous media by the variational-based homogenization method. For no loss of generality, this established criterion is expressed in a consistent form for different cyclic loadings distinguished by the stress ratio $-1 \leq R < 1$.

The following remarks can be concluded:

- The established fatigue criteria are separated into two parts, depending naturally on the sign of J_{3+} . Similar to the Gurson-like limit analysis [7, 9] and the recent statical shakedown approach [69] of porous media in the framework of micromechanics, the symmetry property of the obtained criteria is both with the sign change of Σ_m and that of J_{3+} : $\mathcal{F}(\Sigma_m, \Sigma_{eq}, J_{3+}) = \mathcal{F}(-\Sigma_m, \Sigma_{eq}, -J_{3+})$ in this work. This observation is plotted in Fig.2 by substituting $(\Sigma_\rho - \Sigma_z)_+$ for Σ_{eq+} .
- The obtained fatigue criterion has some analogies with that derived from Melan's statical theorem and presented in the previous study [67]. However, the derivation procedure in this paper using the variational principle does not need to consider the residual stress field due to the choice of kinematical approach. The accuracy of the established criteria relies on the applied fictitious elastic stress field σ^E and the plastic strain rate field $\dot{\epsilon}^p$.
- The application of Dirac's measure (71) is an essential step to simplify the calculation. The volume integral of the local work rate by external actions is accordingly avoided. Actually, concerning the bounded measures techniques [63] (including regular and singular measures), the singular measures are typically associated to alternating plasticity collapses, for which the plastic strain increment shall vanish. For the same reason, the obtained criterion can only provide the limit surface of the alternating plasticity collapse (fatigue). This will be further discussed in the following section.

4. Assessment of the predictive capability of the established criterion

A macroscopic fatigue criterion of porous materials has been obtained in Section 3 by applying the variational principle. For a wide assessment of the predictive capability of the new criterion, comparisons to numerical computations by non-linear optimizations and to analytical results in the previous studies are presented in this section.

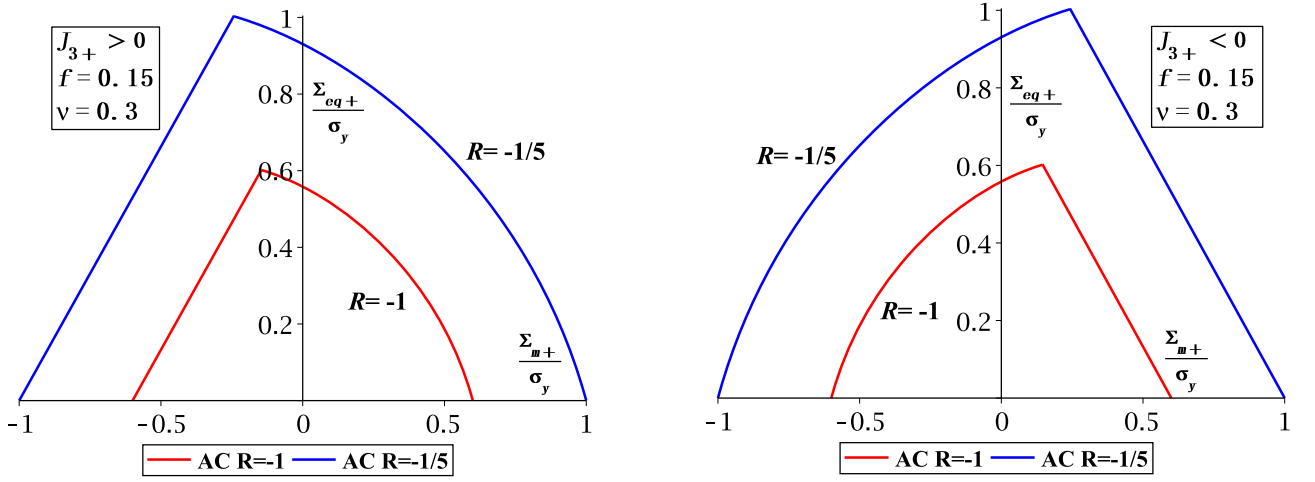


Figure 1: Limit surfaces defined by the analytical criteria (AC) subjected to alternating $R = -1$ (Red line) and intermediate $R = -1/5$ (Blue line) loadings for porosity $f = 0.15$ with Poisson's ratio $\nu = 0.3$ by respect to the sign of J_{3+} (Left: $J_{3+} > 0$; Right: $J_{3+} < 0$).

Fig.1 presents the limit surface defined by the proposed criteria with porosity $f = 0.15$ and Poisson's ratio $\nu = 0.3$ for alternating ($R = -1$) and an intermediate loading ($R = -1/5$) cases. It is obviously seen that the shakedown domain are bounded by two distinct parts, related to the two opposite signs of $J_{3+} > 0$ and $J_{3+} < 0$

For the purpose of exhibiting the symmetric property of the limit surfaces reflecting the effects of the sign of J_{3+} as discussed before, $\mathcal{F}^{(+)}$ and $\mathcal{F}^{(-)}$ are plotted on Fig.2 by substituting $(\Sigma_\rho - \Sigma_z)_+$ for Σ_{eq+} , where $(\Sigma_\rho - \Sigma_z)_+ > 0$ and $(\Sigma_\rho - \Sigma_z)_+ < 0$ are directly related to the ones of $J_{3+} > 0$ and $J_{3+} < 0$. It can be seen that the limit surfaces of the shakedown domain present the symmetric property $\mathcal{F}(\Sigma_m, \Sigma_{eq}, J_3) = \mathcal{F}(-\Sigma_m, \Sigma_{eq}, -J_3)$ as discussed in the previous section. To avoid the repetition, only $\mathcal{F}^{(+)}$ is considered in the following part of this paper for the validation by comparison to numerical results.

4.1. Investigations of the established macroscopic criterion by comparison to numerical results

The implementation of the numerical program consists of two steps: (i) producing the elastic responses under referential load by Finite Element Method; (ii) solving the non-linear optimization problem based on Melan's theorem.

Only a quarter of the REV is taken into consideration due to its geometrical symmetry, which is discretized by 1500 quadratic axisymmetric elements (see Fig.3). The velocity field $\mathbf{v} = \mathbf{D} \cdot \mathbf{x}$ on the exterior boundary of the hollow sphere to prescribe a constant macroscopic stress triaxiality ($T = \Sigma_m / \Sigma_{eq}$) during the load cycles by a user subroutine Multi-Points Constraints (MPC) in Abaqus software [54], which was firstly provided by Cheng and Guo [10] and successfully applied in many studies [12, 5, 6, 51].

Hence, the elastic response $\boldsymbol{\sigma}_0^E(\mathbf{x}_g)$ at each Gauss point \mathbf{x}_g in the unit cell under a reference load Σ_0 can be calculated by using Abaqus/Standard code. Then, for each Gauss

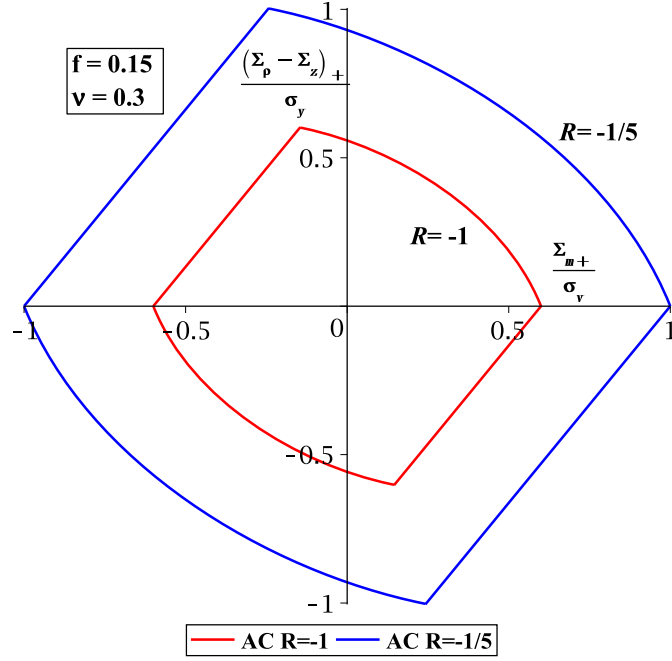


Figure 2: Symmetric shakedown domain for porosity $f = 0.15$ with Poisson's ratio $\nu = 0.3$ defined by the proposed criteria (AC) under alternating $R = -1$ (Red line) and intermediate $R = -1/5$ (Blue line) loadings. Two subfigures on Fig.1 are plotted by substituting $(\Sigma_\rho - \Sigma_z)_+$ for Σ_{eq+} .

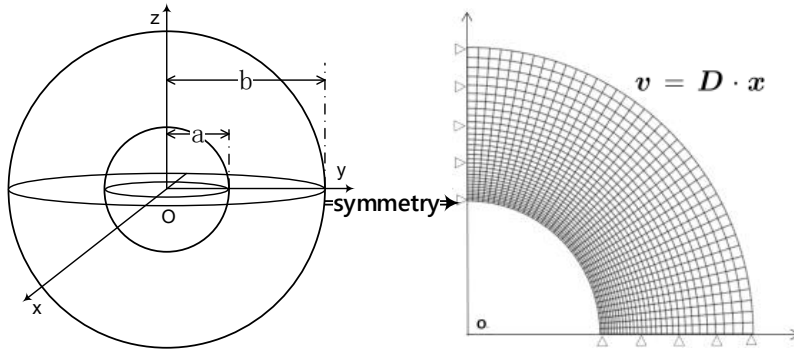


Figure 3: Symmetric hollow sphere representative model with inner and outer radius: a and b , and considered initial FEM mesh . The velocity field $\mathbf{v} = \mathbf{D} \cdot \mathbf{x}$ is imposed at $r = b$.

point \mathbf{x}_g , the computation of the local shakedown load factor α_g is transformed to solving a non-linear optimization problem with respect to different stress ratio:

$$\max_{\alpha_g, \bar{\rho}(\mathbf{x}_g)} \left\{ \alpha_g \quad s.t. \quad \begin{cases} F(\alpha_g \frac{1}{1-R} \sigma_0^E(\mathbf{x}_g) + \bar{\rho}(\mathbf{x}_g), \sigma_y) \leq 0 \\ F(\alpha_g \frac{R}{1-R} \sigma_0^E(\mathbf{x}_g) + \bar{\rho}(\mathbf{x}_g), \sigma_y) \leq 0 \end{cases} \right\} \quad (60)$$

The plastic shakedown limit load factor α_{SD} is obtained as the minimum value of α_g for all the Gauss points \mathbf{x}_g in the considered body. The plastic shakedown limit load is $\Sigma_{SD} = \alpha_{SD} \Sigma_0$ due to the linearity behaviour. Moreover, the first occurrence of fatigue can also be provided by such numerical procedure.

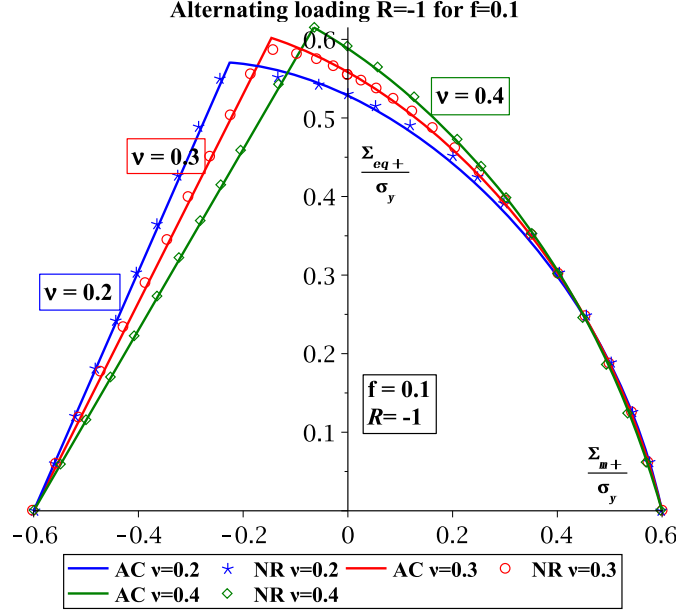


Figure 4: Comparison between the limit surfaces of the analytical criteria (AC) and numerical results (NR) for porosity $f = 0.1$ under alternating loadings $R = -1$ with respect to different values of Poisson's ratio of matrix: $\nu = 0.2$ (Blue), 0.3 (Red) and 0.4 (Green).

Fig.4 and 5 plot the limit surfaces computed from the established macroscopic fatigue criterion and the numerical results under alternating loading ($R = -1$) for the void volume fractions $f = 0.1$ and 0.25 with respect to different Poisson's ratios. A very good agreement between the analytical and numerical results can be observed. Particularly, for the pure hydrostatic case ($\frac{\Sigma_{eq+}}{\sigma_y} = 0$), the numerical results coincide exactly with theoretical predictions $\frac{\Sigma_{m\pm}}{\sigma_y} = \pm \frac{4}{3}(1 - f)$, since both the elastic stress and the plastic strain rate field is obtained from the exact solution. The value of ν has no influence on the plastic shakedown limit in this case.

However, concerning the loading cases with high values of stress triaxiality, small differences between the analytical and numerical results are observed. This can be firstly explained by that the homogeneous stress field (32) used to derive the deviatoric part of the trial plastic strain rate satisfies the boundary condition only in the average manner (33). Besides, errors also originate from the trial elastic stress field under pure deviatoric load (21) obtained by the semi-analytical method.

The influence of Poisson's ratio ν on the macroscopic fatigue criterion can also be studied on Fig.4 and 5. It can be seen that, with the increase of ν , the crossing point of two surfaces defined by Eq.(54) and (56) approaches Σ_{eq+} -axis. Moreover, the macroscopic criteria shrink

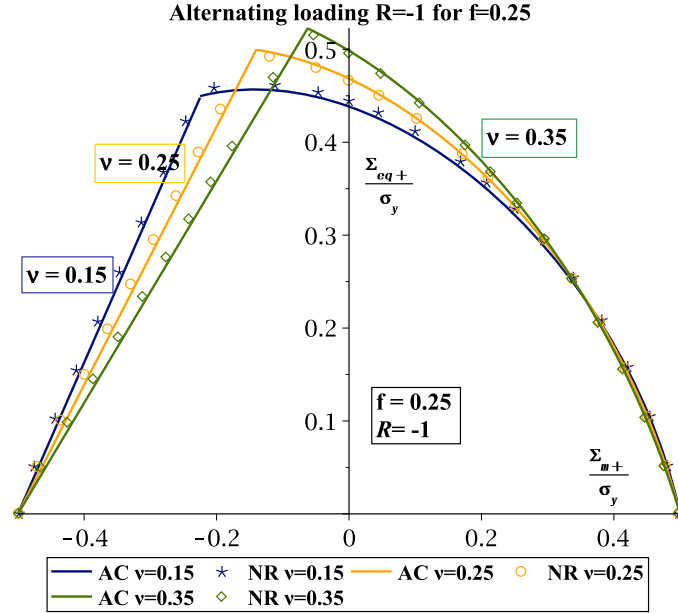


Figure 5: Comparison between the limit surfaces of the analytical criteria (AC) and numerical results (NR) for porosity $f = 0.25$ under alternating loadings $R = -1$ with respect to different values of Poisson's ratio of matrix: $\nu = 0.15$ (Navy), 0.25 (Orange) and 0.35 (Leaf green).

slightly with the variation of ν within the right part, while the shakedown domain in the
405 left part deduces with the increase of ν .

For completeness, the validation for porosity $f = 0.01, 0.2, 0.15$ and 0.3 are also provided in Appendix D. The same conclusions can be made from the comparisons.

Additionally, step-by-step computations to analyse the transient phase before collapse are also performed to verify the assumption in the analytical solution. Fig.6 illustrates
410 the distribution of equivalent stress of the considered model subjected to 50 cycles cyclic loadings with respect to the variation of triaxiality. It can be seen that the maximum value of the equivalent stress always presents on the void surface ($r = a$), and move from the equator to the pole with the decrease of T . Consequently, the supposed "dangerous point" to ensure the shakedown condition (49) is validated. The local strain-stress curve tends to
415 a linear response at the very point and a stabilized cycle with zero width can be observed when shakedown occurs as shown on Fig.7.

On the other hand, Fig.8 and 9 display the comparisons between analytical results and numerical ones of the macroscopic fatigue limit under pulsating $R = 0$ and the intermediate
420 $R = 1/5$ loadings with respect for $f = 0.1$ and 0.2 . It is remarked that the effective safety domain (plotted by the solid line) is at the intersection of the domain defined by the limit surface of the proposed macroscopic fatigue criterion and the one of stress-based limit analysis by [53], which is corresponding to the collapse by development of a mechanism (incremental collapse) at the first cycle.

Recalling the assumption of vanishing plastic strain increment (40) over a stabilized

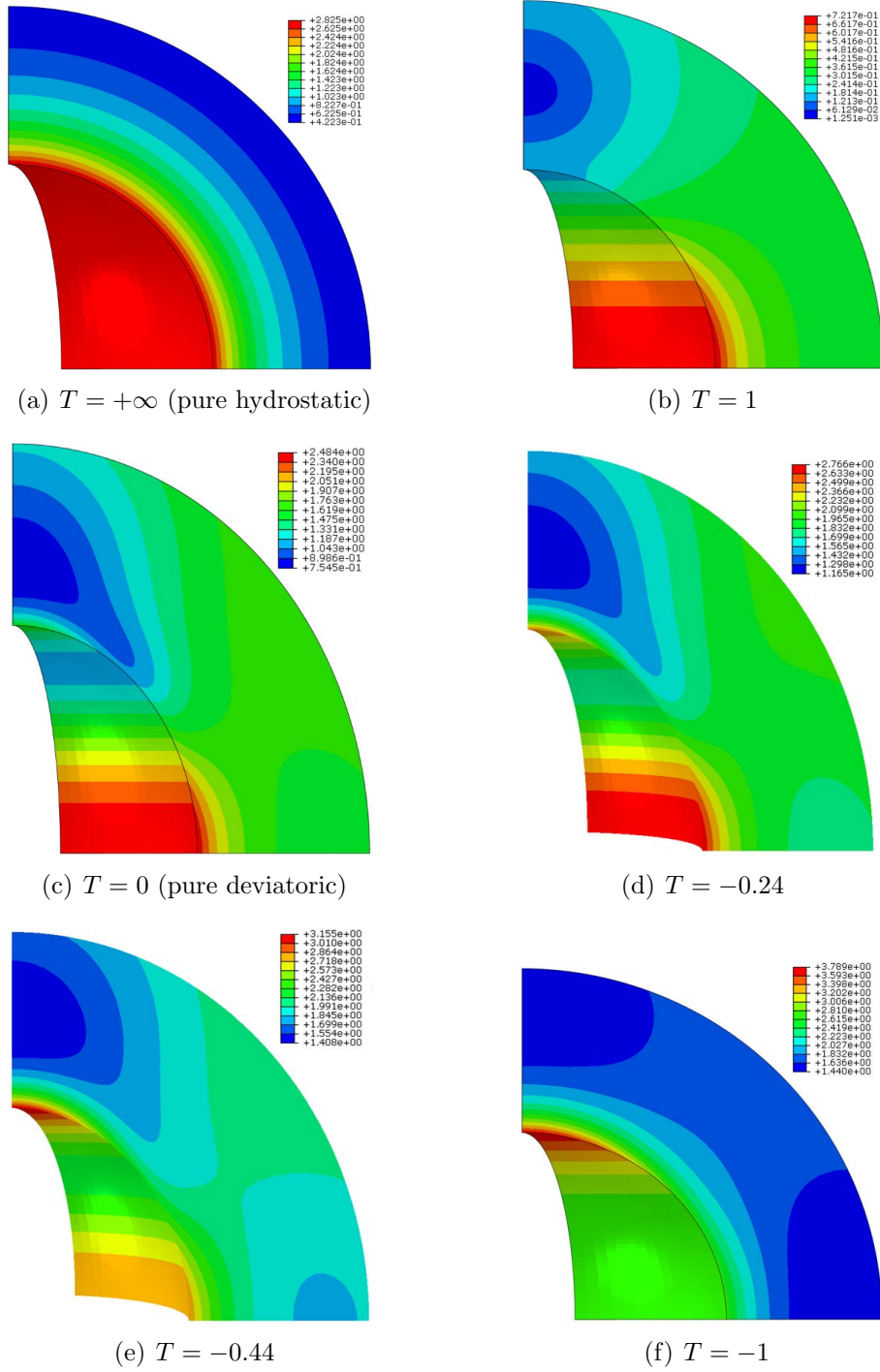


Figure 6: Distribution of equivalent stress σ_{eq} after 50 cycles of cyclic loadings with respect to variation of triaxiality T : (a) $T = +\infty$; (b) $T = 1$; (c) $T = 0$; (d) $T = -0.24$; (e) $T = -0.44$; (f) $T = -1$. The maximum value of the equivalent stress always presents on the void surface ($r = a$).

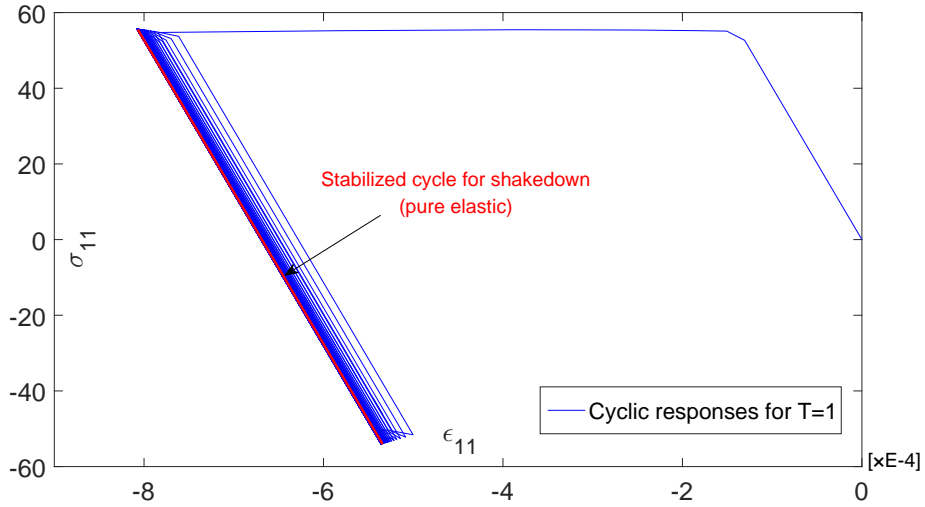


Figure 7: Cyclic responses $\epsilon_{11}-\sigma_{11}$ on the internal boundary ($r = a$) at $\theta = \pi/2$ by step-by-step computations for traxiality $T = 1$. Porosity $f = 0.15$ and Poisson's ratio $\nu = 0.25$ are adopted. The cyclic responses tend to purely elastic when shakedown occurs.

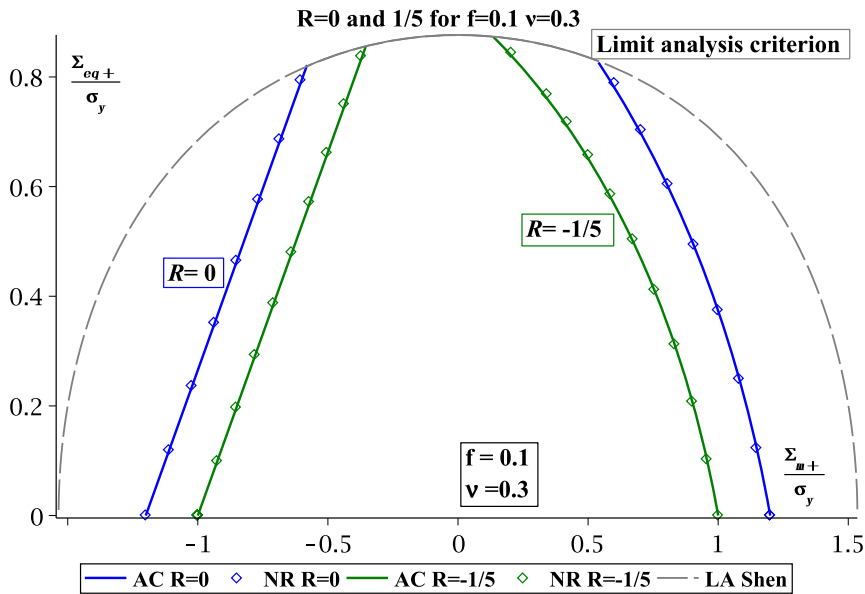


Figure 8: Comparison between the analytical criteria (AC, solid line) and numerical results (NR, diamond) for porosity $f = 0.1$ with Poisson's ratio $\nu = 0.3$ under pulsating $R = 0$ (Blue) and intermediate $R = -1/5$ (Green) loadings. The gray dash line represents the limit analysis criterion (LA) proposed in [53].

425 cycle, only the mechanism of alternating plasticity collapse is considered in the derivation in order to apply the Dirac's measure. While concerning the incremental collapse, for which the increment of plastic strain is nonzero, the mechanisms of failure can not be predicted by the proposed criteria. The new fatigue criteria are computed by maximizing the amplitude

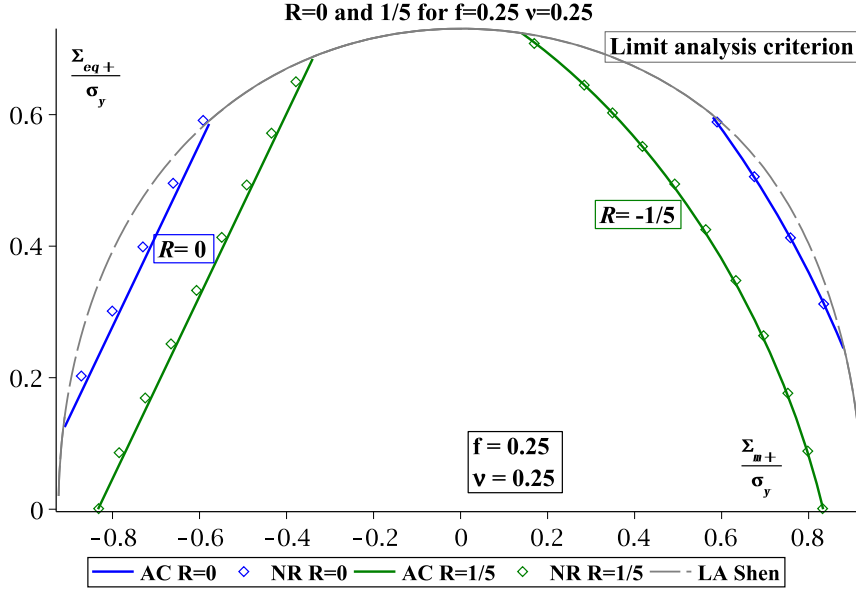


Figure 9: Comparison between the analytical criteria (AC, solid line) and numerical results (NR, diamond) for porosity $f = 0.25$ with Poisson's ratio $\nu = 0.25$ under pulsating $R = 0$ (Blue) and intermediate $R = -1/5$ (Green) loadings. The gray dash line represents the limit analysis criterion (LA) proposed in [53].

of cyclic loadings. Obviously, an additional constraint of the maximum proportional load is required to ensure the material's safety. Consequently, the shakedown domain for high values of T is bounded by the limit analysis criterion [53] as shown on Fig.8 and 9. The failure due to excessive deformation at the first cycle will immediately arrive in this case (e.g. for triaxiality $T = 0$ under pulsating loadings $R = 0$ on Fig.8).

On the contrary, regarding Fig.15 to Fig.18, the collapse by such mechanism does not occur for alternating loading case. Thus, the safety domain is only defined by the proposed fatigue criterion. The effective shakedown criterion is found much smaller and completely inside the one under monotonic loads.

4.2. Comparisons to analytical criteria in previous study and discussions

In this subsection, the new macroscopic fatigue criterion is compared with the quasi-lower bound proposed in [67] based on Melan's classical theorem under pulsating and alternating loadings.

Fig.10 to Fig.12 illustrate the comparison of the new macroscopic criterion (AC), the previous one (LB) and the numerical results (NR) for the alternating ($R = -1$) and pulsating loading ($R = 0$) cases with the porosities $f = 0.01, 0.1$ and 0.2 , respectively. As mentioned before, it is clearly seen that the two criteria derived from the different approaches both preserve the exact solution of the hollow sphere subjected hydrostatic loadings.

The noticeable differences between the quasi-lower approach in [67] and the numerical results for large porosities (Fig.11 and 12) are obviously improved by the new fatigue criteria established in this paper. The reason is that the errors due to the approximated

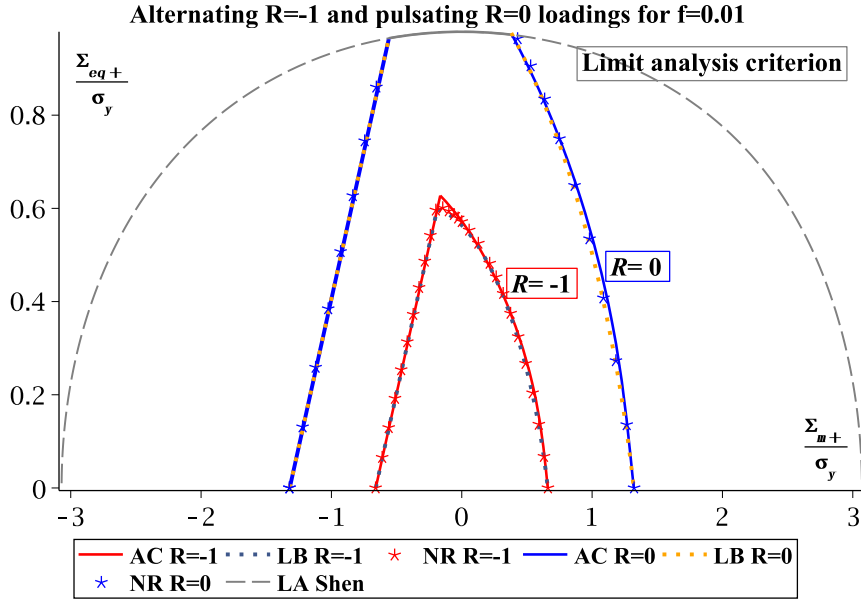


Figure 10: Comparisons between the established criteria (AC, solid line) and the lower bound (LB, dot line) based on Melan’s theorem given in [67] for porosity $f = 0.01$ under alternating (Red) and pulsating (Blue) loadings. Gray dash line: limit analysis criterion (LA) proposed in [53]; Asterisk: numerical results (NR).

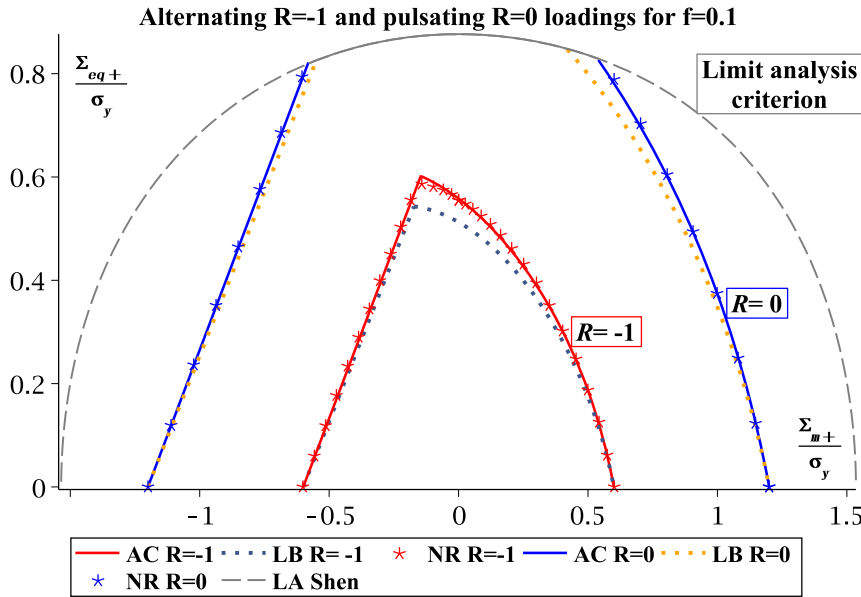


Figure 11: Comparisons between the established criteria (AC, solid line) and the lower bound (LB, dot line) based on Melan’s theorem given in [67] for porosity $f = 0.1$ under alternating (Red) and pulsating (Blue) loadings. Gray dash line: limit analysis criterion (LA) proposed in [53]; Asterisk: numerical results (NR).

450 time-independent residual stress field, the key idea of Melan’s theorem, is prevented in the present research, since such a residual stress field is not required by the variational-based

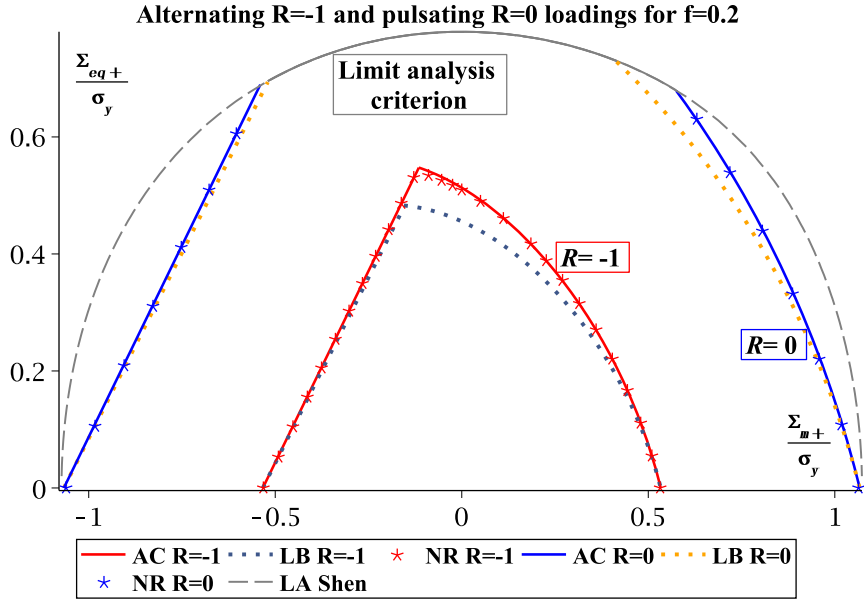


Figure 12: Comparisons between the established criteria (AC, solid line) and the lower bound (LB, dot line) based on Melan’s theorem given in [67] for porosity $f = 0.2$ under alternating (Red) and pulsating (Blue) loadings. Gray dash line: limit analysis criterion (LA) proposed in [53]; Asterisk: numerical results (NR).

homogeneous model. Moreover, the new trial fictitious elastic stress field under pure deviatoric load is correspondingly much richer to capture the main shear effects of the hollow sphere with more terms.

455 Meanwhile, the new criteria do not present a sufficient accurate prediction of the shakedown domain for small porosity $f = 0.01$ around the deviatoric part (Fig.10). According to the Cheng et al. [9], for small porosities, large plastic strain heterogeneities may occur in the vicinity of the void surface. Thus, the adopted trial homogeneous stress field which is relaxed on the boundary condition leads to this inaccuracy.

460 5. Conclusions

In this paper, we have developed a new variational homogenization method to determine macroscopic fatigue criteria of porous materials under general cyclic conditions. Different from the previous studies, the proposed homogeneous model is on account of the equivalence between the plastic dissipation and the external work rate in nature over a stabilized cycle. 465 With this new method, it is no more needed to consider the time-independent residual stress field, which is a laborious task in the classical Melan’s theorem.

A specific macroscopic fatigue criterion has been established by using the new variational method for porous materials with a von Mises type solid matrix and for a large range of porosity. This criterion is expressed as a closed-form function of the first two stress invariants of macroscopic stress tensor Σ_m and Σ_{eq} , the sign of the third one J_3 , Poisson’s ratio and void volume fraction. The corresponding safety domain is defined by the proposed fatigue 470

criteria and the yield strength based on limit analysis for some specific loading conditions.

The established new criterion has been assessed by comparing the theoretical predictions of limit states with some analytical solutions and with numerical results from direct simulations of the hollow sphere. The accuracy of the new criterion has been clearly demonstrated. Especially for materials with large values of porosity, the new criterion significantly improves the prediction of the plastic shakedown limit load with respect to the previous studies.

Finally, it is worth noticing that in this paper, the von Mises type solid matrix is considered for metal porous materials. As future prospectives, a challenging topic is to consider the non-associated plastic Drucker-Prager solid matrix by using the bipotential theory for porous materials in geomechanics engineering.

Acknowledgements

The authors would like to thank the National Natural Science Foundation of China (Grant No.11902111) and the Fundamental Research Funds for the Central Universities (Grant No.B210202045).

Appendix A Application of De Saxcé's solution to hollow sphere under isotropic pressure

The idea of using Markov's principle over a cycle (13) was initially proposed by Save et al. [49] and applied on the thick wall tube subjected to isotropic pressure. The derivation is briefly rewritten in order to be implemented in the shakedown analysis of the porous materials under pure hydrostatic loadings in the following part.

Let us consider a hollow sphere under uniform pressure p upon its outer boundary $\partial\Omega$. Taking into account the central symmetry of the problem, it is easy to obtain the elastic solution in the fictitious elastic body within the spherical coordinates $\{\mathbf{e}_r, \mathbf{e}_\theta, \mathbf{e}_\phi\}$:

$$\boldsymbol{\sigma}^E = \frac{p}{1-f} \left(\mathbf{1} + \frac{1}{2} \left(\frac{a}{r} \right)^3 (\mathbf{e}_\theta \otimes \mathbf{e}_\theta + \mathbf{e}_\phi \otimes \mathbf{e}_\phi - 2 \mathbf{e}_r \otimes \mathbf{e}_r) \right) \quad (61)$$

Beyond the elastic region for von Mises model, one can build the following relation due to the spherical symmetry:

$$\sigma_{\varphi\varphi} = \sigma_{\theta\theta} \quad (62)$$

Furthermore, considering the normality law (2) and the yield condition (18), the following equation can be built:

$$\dot{\varepsilon}_{rr}^p(r) = -\frac{1}{2} \dot{\varepsilon}_{\varphi\varphi}^p(r) = -\frac{1}{2} \dot{\varepsilon}_{\theta\theta}^p(r) \quad (63)$$

for the nonzero components of the plastic strain rate field.

The equivalent strain rate is calculated as follows:

$$\varepsilon_{eq}(\dot{\boldsymbol{\varepsilon}}^p) = \sqrt{\frac{2}{3} \dot{\boldsymbol{\varepsilon}}^p : \dot{\boldsymbol{\varepsilon}}^p} = |\dot{\varepsilon}_{rr}^p| \quad (64)$$

Besides, taking account of normality law, it is readily seen:

$$\boldsymbol{\sigma} : \dot{\boldsymbol{\varepsilon}}^p \leq \sigma_{eq}(\boldsymbol{\sigma}) \varepsilon_{eq}(\dot{\boldsymbol{\varepsilon}}^p) \leq \sigma_y \varepsilon_{eq}(\dot{\boldsymbol{\varepsilon}}^p) \quad (65)$$

Thus, the plastic dissipation function of von Mises model is reduced to:

$$\mathcal{D}(\dot{\boldsymbol{\varepsilon}}^p) = \sigma_y |\dot{\varepsilon}_{rr}^p| \quad (66)$$

Consequently, applying the established minimum function (17) to the shakedown problem of hollow sphere under isotropic loadings leads to

$$\int_{\Omega} \oint \sigma_y |\dot{\varepsilon}_{rr}^p| dt dV - \int_{\Omega} \oint \left(\frac{3}{2} \frac{p}{1-f} \left(\frac{a}{r} \right)^3 \dot{\varepsilon}_{rr}^p \right) dt dV = 0 \quad (67)$$

505 Assuming that the collapse occurs by alternating plasticity (fatigue) in a stabilized cycle of a unit period, the admissible plastic strain increment reads:

$$\Delta \varepsilon_{rr}^p = \oint \dot{\varepsilon}_{rr}^p dt = \dot{\varepsilon}_{rr+}^p + \dot{\varepsilon}_{rr-}^p = 0 \quad (68)$$

where $\dot{\varepsilon}_{rr+}^p$ (resp. $\dot{\varepsilon}_{rr-}^p$) is a constant value of the radial plastic strain rate, corresponding to the applied pressure reaching its maximal value p_+ (resp. minimal value p_-) in the limit state. So the shakedown condition (67) rewrites:

$$\int_{\Omega} \sigma_y (|\dot{\varepsilon}_{rr+}^p| + |\dot{\varepsilon}_{rr-}^p|) dV - \int_{\Omega} \left(-\frac{3}{2} \frac{p_+ \dot{\varepsilon}_{rr+}^p - p_- \dot{\varepsilon}_{rr-}^p}{1-f} \left(\frac{a}{r} \right)^3 \right) dV = 0 \quad (69)$$

510 and reduces to:

$$\int_a^b 2\sigma_y \dot{\varepsilon}_{rr+}^p r^2 dr - \int_a^b \left(\frac{3}{2} \frac{(p_+ - p_-) \dot{\varepsilon}_{rr+}^p}{1-f} \left(\frac{a}{r} \right)^3 \right) r^2 dr = 0 \quad (70)$$

In order to simplify the computation, the bounded measures technique [62] is adopted: if x_0 belongs to Ω and δ_{x_0} is a linear form on the space of the continuous functions, Dirac's measure, the simplest case of non regular measures, is written as

$$\int \delta_{x_0}(x) \phi(x) d\Omega = \phi(x_0) \quad (71)$$

which is bounded by

$$\|\delta_{x_0}\| = 1 \quad (72)$$

515 It is proved that the admissible plastic strain rate field $\dot{\boldsymbol{\varepsilon}}^p$ in the hollow sphere always converges to Dirac's measure concerning shakedown problem, which allows to eliminate the volume integral.

As for the isotropic loads, the plastic yielding occurs in a small ring at $r = c$ ($a \leq c \leq b$), then Dirac's distribution $\delta(r - c)$ can be expressed by

$$\int_a^b \delta(r - c) \phi(r) 4\pi r^2 dr = \phi(c) \quad (73)$$

520 so that the integral in (70) can be simplified:

$$2\sigma_y \dot{\varepsilon}_{rr+}^p c^2 - \frac{3}{2} \frac{(p_+ - p_-) \dot{\varepsilon}_{rr+}^p}{1 - f} \left(\frac{a}{c}\right)^3 c^2 = 0 \quad (74)$$

The shakedown condition is fulfilled with the cycle amplitude $\Delta p = p_+ - p_-$:

$$\Delta p = \frac{4}{3}(1 - f) \left(\frac{a}{c}\right)^3 \sigma_y \quad (75)$$

In the homogenization study of porous media, the macroscopic mean stress can be calculated owing to (4) and (61)

$$\Sigma_m = \frac{1}{3} \text{tr}(\Sigma(p)) = p \quad (76)$$

525 The maximal value of $\Delta\Sigma_m$ is reached for $c = a$. Hence, the amplitude of the plastic shakedown limit load is

$$\Delta\Sigma_m^{SD} = \frac{4}{3}(1 - f)\sigma_y \quad (77)$$

530 It is worthy remarking that the obtained result of the plastic shakedown limit load coincides to the one in [68] by Melan's statical theorem, indicating that it is the exact solution for the pure hydrostatic loading case. Indeed, in the framework of shakedown analysis (or limit analysis), the minimization problem from the variational formulation (e.g. Eq.(16)) can be solved if the exact velocity or stress field is provided.

Appendix B Determination of the proposed trial elastic stress filed under pure deviatoric loadings

535 The general solution for a hollow sphere subjected to axisymmetric deviatoric loadings is a combination of the so-called internal and external problems inspired from the Papkovitch-Neuber formulations [55]. The problem is divided into a solid sphere subjected to an axisymmetric traction exerted onto its boundary ($r = b$) and a spherical hole embedded in an infinite solid (The radius of cavity is noted as $r = a$) with vanishing loading at infinity.

The general solution in terms of Legendre's polynomial series in the spherical frame is

given by:

$$\begin{aligned}
\sigma_{rr}^E &= 2M_0 \sum_n \left[A_n (n+1) (n^2 - n - 2 - 2\nu) r^n + B_n n (n-1) r^{n-2} \right. \\
&\quad \left. - \frac{C_n}{r^{n+1}} n (n^2 + 3n - 2\nu) + \frac{D_n}{r^{n+3}} (n+1) (n+2) \right] P_n(\zeta) \\
\sigma_{r\theta}^E &= 2M_0 \sum_n \left[A_n (n^2 + 2n - 1 + 2\nu) r^n + B_n (n-1) r^{n-2} \right. \\
&\quad \left. - \frac{C_n}{r^{n+1}} (n^2 - 2 + 2\nu) - \frac{D_n}{r^{n+3}} (n+2) \right] \frac{d}{d\theta} P_n(\zeta) \\
\sigma_{\theta\theta}^E &= 2M_0 \sum_n \left[-A_n (n^2 + 4n + 2 + 2\nu) (n+1) r^n - B_n n^2 r^{-2} \right. \\
&\quad \left. + \frac{C_n}{r^{n+1}} n (n^2 - 2n - 1 + 2\nu) - \frac{D_n}{r^{n+3}} (n+1)^2 \right] P_n(\zeta) + 2M_0 \sum_n \left[-B_n r^{n-2} \right. \\
&\quad \left. - A_n (n+5 - 4\nu) - \frac{C_n}{r^{n+1}} (-n+4 - 4\nu) - \frac{D_n}{r^{n+3}} \right] \cot \theta \frac{d}{d\theta} P_n(\zeta) \\
\sigma_{\varphi\varphi}^E &= 2M_0 \sum_n \left[A_n (n-2 - 2\nu - 4\nu n) (n+1) r^n + B_n n r^{-2} \right. \\
&\quad \left. + \frac{C_n}{r^{n+1}} n (n+3 - 2\nu - 4\nu n) - \frac{D_n}{r^{n+3}} (n+1) \right] P_n(\zeta) + 2M_0 \sum_n \left[B_n r^{n-2} \right. \\
&\quad \left. + A_n (n+5 - 4\nu) + \frac{C_n}{r^{n+1}} (-n+4 - 4\nu) + \frac{D_n}{r^{n+3}} \right] \cot \theta \frac{d}{d\theta} P_n(\zeta)
\end{aligned} \tag{78}$$

540 where A_n, B_n, C_n, D_n are 4 sets of constants to be determined.

Considering the standard Legendre equation with the new variable $\zeta = \cos \theta$, the Legendre polynomials of the first kind $P_n(\zeta)$ for $|\zeta| \leq 1$ is obtained as:

$$P_n(\zeta) = \frac{1}{2^n n!} \frac{d^n (\zeta^2 - 1)}{d\zeta^n} \tag{79}$$

We claim that the new trial elastic stress field $\boldsymbol{\sigma}^E$ is statically admissible (5) in the following way:

545 • $\boldsymbol{\sigma}^E$ satisfies the internal equilibrium equations in spherical coordinates:

$$\begin{aligned}
\frac{\partial \sigma_{rr}}{\partial r} + \frac{1}{r} \frac{\partial \sigma_{r\theta}}{\partial \theta} + \frac{1}{r \sin \theta} \frac{\partial \sigma_{r\varphi}}{\partial \varphi} + \frac{1}{r} (2\sigma_{rr} - \sigma_{\theta\theta} - \sigma_{\varphi\varphi} + \sigma_{r\theta} \cot \theta) &= 0 \\
\frac{\partial \sigma_{r\theta}}{\partial r} + \frac{1}{r} \frac{\partial \sigma_{\theta\theta}}{\partial \theta} + \frac{1}{r \sin \theta} \frac{\partial \sigma_{\theta\varphi}}{\partial \varphi} + \frac{1}{r} ((\sigma_{\theta\theta} - \sigma_{\varphi\varphi}) \cot \theta + 3\sigma_{r\theta}) &= 0 \\
\frac{\partial \sigma_{\varphi r}}{\partial r} + \frac{1}{r} \frac{\partial \sigma_{\varphi\theta}}{\partial \theta} + \frac{1}{r \sin \theta} \frac{\partial \sigma_{\varphi\varphi}}{\partial \varphi} + \frac{1}{r} (3\sigma_{r\theta} + 2\sigma_{\theta\varphi}) &= 0
\end{aligned} \tag{80}$$

• Concerning the free stress on the void surface:

$$\boldsymbol{\sigma}^E \cdot \underline{n} = \mathbf{0} \tag{81}$$

Thus,

$$\sigma_{rr}^E(r = a, \theta) = 0, \quad \sigma_{r\theta}^E(r = a, \theta) = 0 \quad (82)$$

It is verified that the internal equilibrium condition (80) is auto-satisfied with the general form (78). Besides, following [55], the only term for $n = 2$ of the involved Legendre's polynomial series is not vanishing in this case. Then, the polynomial of degree 2 is obtained by a simple identification:

$$P_2(\zeta) = \frac{1}{2}(3 \cos^2 \theta - 1) \quad (83)$$

As a result, the previous conditions for the proposed elastic stress field are reduced to

$$\begin{cases} -6A_2\nu f^{2/3} + 2B_2 - 2(10 - 2\nu) \frac{C_2}{f} + \frac{12D_2}{f^{5/3}} = 0 \\ (7 + 2\nu) A_2 f^{2/3} + B_2 - (2 + 2\nu) \frac{C_2}{f} - 4 \frac{D_2}{f^{5/3}} = 0 \end{cases} \quad (84)$$

Solving the previous equations, one has:

$$\begin{cases} B_2 = -\frac{21}{5} 21A_2 f^{2/3} - 2C_2 \nu f^{-1} + \frac{14}{5} C_2 f^{-1} \\ D_2 = \frac{1}{2} A_2 \nu f^{7/3} + \frac{7}{10} A_2 f^{7/3} + \frac{6}{5} C_2 f^{2/3} \end{cases} \quad (85)$$

Considering the definition of the average stress (4), the macroscopic stress tensor writes:

$$\Sigma = M_0 \frac{\frac{56}{5} f^{5/3} A_2 - \frac{56}{5} A_2 + \frac{8}{3} f B_2 - \frac{8}{3} B_2}{\frac{4}{3}} \begin{bmatrix} 1 & 0 & 0 \\ 0 & 1 & 0 \\ 0 & 0 & -2 \end{bmatrix} \quad (86)$$

Applying to (44) for the pure deviatoric alternating loading case ($\Sigma_m = M_1 = 0$ and $R = -1$) leads to

$$\Sigma_{eq+} = \frac{4(21A_2 f^{5/3} + 5B_2 f - 21A_2 - 5B_2) f^{5/3}}{5(8A_2 f^{7/3} \nu - 28A_2 f^{7/3} - 4B_2 f^{5/3} + 8C_2 \nu f^{2/3} + 2C_2 f^{2/3} - 9D_2)} \quad (87)$$

Substituting B_2 and D_2 by (85), Eq.(87) is recast to

$$\Sigma_{eq+} = \frac{8}{5} \frac{21A_2 f^{5/3} - 10C_2 \nu f - 21A_2 f + 14C_2 f + 10C_2 \nu - 14C_2}{7A_2 \nu f^{5/3} - 35A_2 f^{5/3} + 32C_2 \nu - 40C_2} \quad (88)$$

The next step is to determine A_2 and C_2 . In consideration of the dependency of the elastic stress field on the porosity and Poisson's ratio, a proposed expression is as follows:

$$\Sigma_{eq+} = a_1 f^{b_1} (c_1 \nu + d_1) + f^{b_2} (c_2 \nu + d_2) + a_3 (c_3 \nu + d_3) \quad (89)$$

The numerical data (reported in Table 1) of the shakedown limit under pure deviatoric alternating loading are obtained by the non-linear optimization method described in Section 4. Non-linear fitting of the shakedown limits with respect to various values of porosity and Poisson's ratio are performed as shown on Fig.13.

Σ_{eq}^E/σ_y	f			
	0.01	0.1	0.2	0.3
ν 0.2	0.5544	0.5302	0.4827	0.4247
0.3	0.5714	0.5557	0.5091	0.4477
0.4	0.5908	0.5907	0.5456	0.4786

Table 1: Numerical values of the shakedown limit under pure deviatoric alternating load.

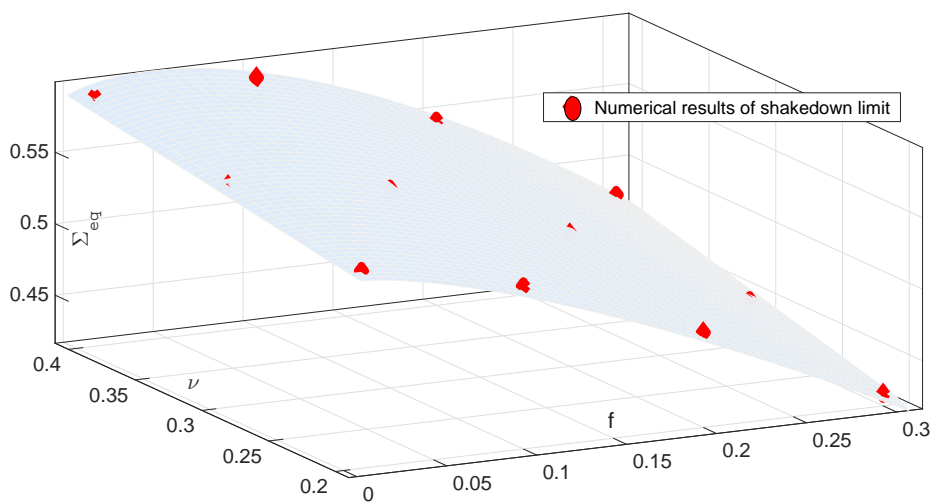


Figure 13: Non-linear fitting of the shakedown limits under pure deviatoric ($T = 0$) and alternating ($R = -1$) loadings extracted from numerical simulations with different porosity $f \in \{0.01, 0.1, 0.2, 0.3\}$ and Poisson's ratio $\nu \in \{0.2, 0.3, 0.4\}$. Gray surface: plotted expression of Σ_{eq} ; Red points: numerical shakedown limits under pure deviatoric loadings.

The parameters in Eq.(89) can be identified:

$$\begin{aligned}
a_1 &= -1.808 & a_3 &= 0.5705 & b_1 &= 1.251 & b_2 &= 1.063 \\
c_1 &= 4.658 & c_2 &= 7.119 & c_3 &= 0.2738 \\
d_1 &= -0.2971 & d_2 &= 0.9803 & d_3 &= 0.917
\end{aligned} \tag{90}$$

Consequently, combining (84), (85), (88) and (89), A_2, B_2, C_2 and D_2 are determined by a simplest solution:

$$\begin{aligned}
A_2 &= -3.85 \cdot 10^8 f^{1.251} \nu^2 + 5.06 \cdot 10^8 f^{1.251} \nu - 3.07 \cdot 10^7 f^{1.251} + 3.25 \cdot 10^8 f^{1.063} \nu^2 - 4.52 \cdot 10^8 f^{1.063} \nu \\
&\quad + 5.60 \cdot 10^7 f^{1.063} + 2.29 \cdot 10^7 \nu f - 3.2 \cdot 10^7 f + 7.14 \cdot 10^6 \nu^2 - 7.87 \cdot 10^6 \nu + 2.11 \cdot 10^6 \\
B_2 &= -1.34 \cdot 10^8 + 2.71 \cdot 10^9 f^{1.918} \nu^2 - 3.37 \cdot 10^9 f^{1.918} \nu - 2.30 \cdot 10^9 f^{1.730} \nu^2 + 3.02 \cdot 10^9 f^{1.730} \nu \\
&\quad - 9.60 \cdot 10^7 f^{1.667} \nu - 1.68 \cdot 10^8 f^{1.918} \nu^3 + 1.42 \cdot 10^8 f^{1.730} \nu^3 + 3.12 \cdot 10^6 \nu^3 f^{0.667} + 1.34 \cdot 10^8 f^{1.667} \\
&\quad - 3.95 \cdot 10^7 f^{0.667} \nu^2 - 1.08 \cdot 10^8 f^{0.667} \nu + 9.60 \cdot 10^7 \nu + 2.04 \cdot 10^8 f^{1.918} - 3.73 \cdot 10^8 f^{1.730} \\
&\quad + 1.99 \cdot 10^8 f^{0.667} \\
C_2 &= 8.42 \cdot 10^7 f^{2.918} \nu^2 - 4.26 \cdot 10^8 f^{2.918} \nu + 2.69 \cdot 10^7 f^{2.918} - 7.12 \cdot 10^7 f^{2.730} \nu^2 + 3.66 \cdot 10^8 f^{2.730} \nu \\
&\quad - 4.90 \cdot 10^7 f^{2.730} - 1.56 \cdot 10^6 f^{1.667} \nu^2 + 2.58 \cdot 10^6 f^{1.667} \nu + 7.42 \cdot 10^7 f^{1.667} - 4.8 \cdot 10^7 f \\
D_2 &= 9.05 \cdot 10^7 f^{2.333} + 3.57 \cdot 10^6 \nu^3 f^{2.333} - 8.10 \cdot 10^5 \nu^2 f^{2.333} + 1.07 \cdot 10^7 f^{3.854} - 1.96 \cdot 10^7 f^{3.396} \\
&\quad - 2.24 \cdot 10^7 f^{3.333} + 1.63 \cdot 10^8 \nu^3 f^{3.396} - 8.34 \cdot 10^7 \nu^2 f^{3.396} + 1.51 \cdot 10^8 \nu f^{3.396} + 1.14 \cdot 10^7 \nu^2 f^{3.333} \\
&\quad + 8.45 \cdot 10^7 f^{3.854} \nu^2 - 1.73 \cdot 10^8 f^{3.854} \nu - 1.36 \cdot 10^6 \nu f^{2.333} - 1.92 \cdot 10^8 \nu^3 f^{3.854} - 5.76 \cdot 10^7 f^{1.667}
\end{aligned} \tag{91}$$

Taking (91) into (78), we obtain the full expression of the new admissible elastic stress field under pure deviatoric load.

The distributions of the equivalent stress σ_{eq} in the solid phase and on the boundaries are plotted on Fig.14. It is remarked that the hollow spherical cell will undergo incipient plastic strains firstly on its inner boundary at equator ($r = a, \theta = \pi/2$) if the load parameter M_0 increases.

Appendix C Formulations of plastic strain rate field derived from (29)

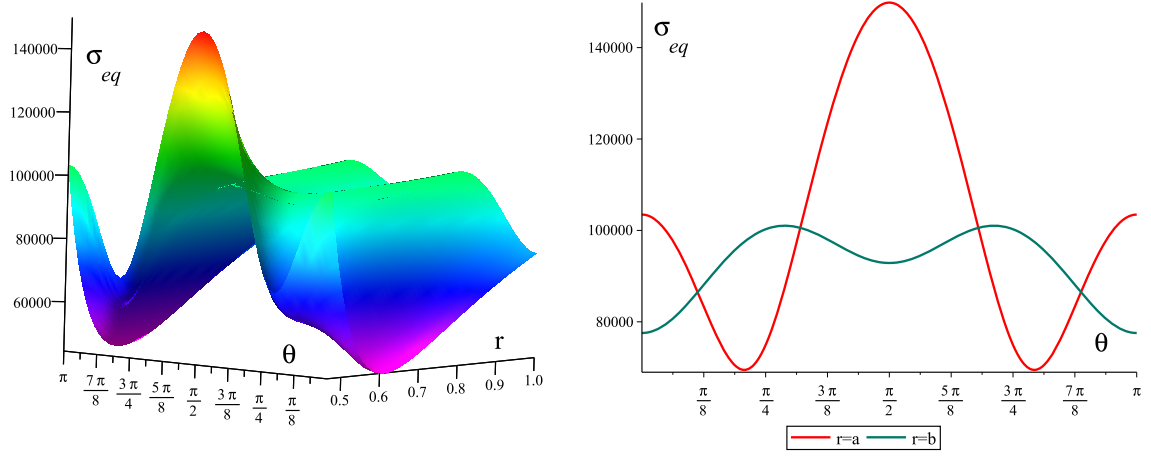
Accounting for the definition $\dot{\boldsymbol{\varepsilon}}^p = \frac{1}{2}(\text{grad} \mathbf{v} + \text{grad}^T \mathbf{v})$, the plastic strain rate field can be obtained derived from the adopted trial velocity field (29) in the spherical coordinates:

$$\begin{aligned}
\dot{\boldsymbol{\varepsilon}}^p &= - \left(2 \frac{G_1}{r^3} + 3G_2(1 + 3 \cos 2\theta) \right) \mathbf{e}_r \otimes \mathbf{e}_r + \left(\frac{G_1}{r^3} + 3G_2(3 \cos 2\theta - 1) \right) \mathbf{e}_\theta \otimes \mathbf{e}_\theta \\
&\quad + \left(\frac{G_1}{r^3} + 6G_2 \right) \mathbf{e}_\phi \otimes \mathbf{e}_\phi + 9G_2 \sin 2\theta (\mathbf{e}_r \otimes \mathbf{e}_\theta + \mathbf{e}_\theta \otimes \mathbf{e}_r)
\end{aligned} \tag{92}$$

which takes the same form with (34).

Then the corresponding equivalent strain rate can be calculated as:

$$\varepsilon_{eq}(\dot{\boldsymbol{\varepsilon}}^p) = 2 \sqrt{\left(\frac{G_1}{r^3} \right)^2 + 3 \frac{G_1}{r^3} G_2 (1 + 3 \cos 2\theta) + 36 G_2^2} \tag{93}$$



(a) 3D plot of equivalent stress distribution σ_{eq} with variation of r and θ . (b) Variation of σ_{eq} on the inner (Red line: $r = a$) and outer (Green line: $r = b$) boundaries.

Figure 14: Contour plots of local equivalent stress σ_{eq} under reference load corresponding to pure deviatoric condition ($T = 0$) with porosity $f = 0.1$ and Poisson's ratio $\nu = 0.3$.

As mentioned in Section 3, we adopt the strain rate field (34) obtained by the normality law from the total stress field. The reason is that the parameters in (34) can be easily eliminated by considering an additional relation of the enforced macroscopic triaxiality (46), although (92) and (93) lead to the same form of the shakedown formulation in (39).

Appendix D Comparison of the macroscopic criteria with numerical results for alternating loading case ($R = -1$)

For completeness, Fig.15 to 18 display the comparisons between analytical results and numerical data of the shakedown limit with respect to $f = 0.01, 0.15, 0.2$ and 0.3 under alternating loadings ($R = -1$).

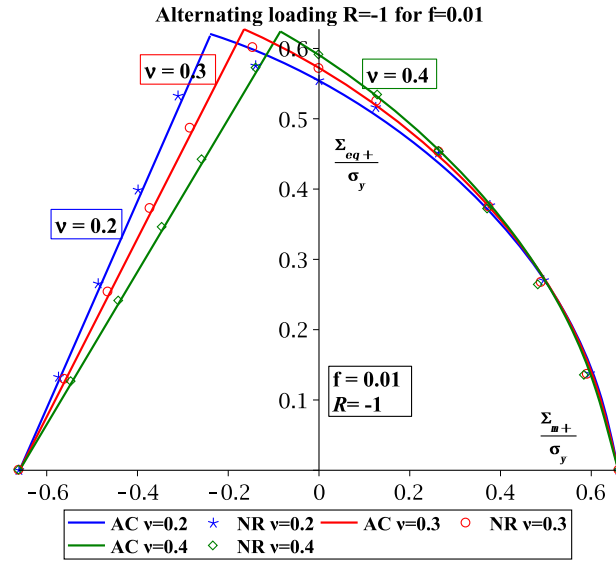


Figure 15: Comparison between the limit surfaces of the analytical criteria (AC) and numerical results (NR) for porosity $f = 0.01$ under alternating loadings $R = -1$ with respect to different values of Poisson's ratio of matrix: $\nu = 0.2$ (Blue), 0.3 (Red) and 0.4 (Green).

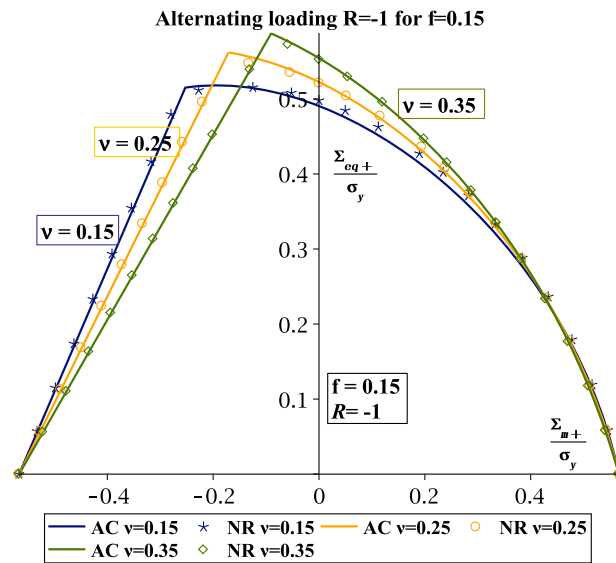


Figure 16: Comparison between the limit surfaces of the analytical criteria (AC) and numerical results (NR) for porosity $f = 0.15$ under alternating loadings $R = -1$ with respect to different values of Poisson's ratio of matrix: $\nu = 0.15$ (Navy), 0.25 (Orange) and 0.35 (Leaf green).

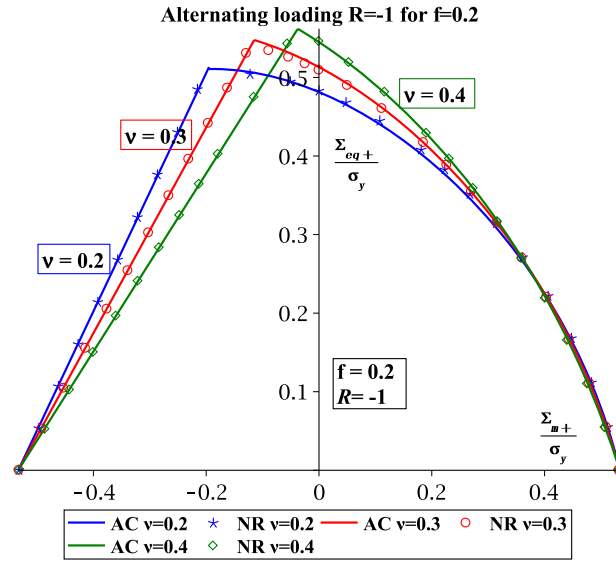


Figure 17: Comparison between the limit surfaces of the analytical criteria (AC) and numerical results (NR) for porosity $f = 0.2$ under alternating loadings $R = -1$ with respect to different values of Poisson's ratio of matrix: $\nu = 0.2$ (Blue), 0.3 (Red) and 0.4 (Green).

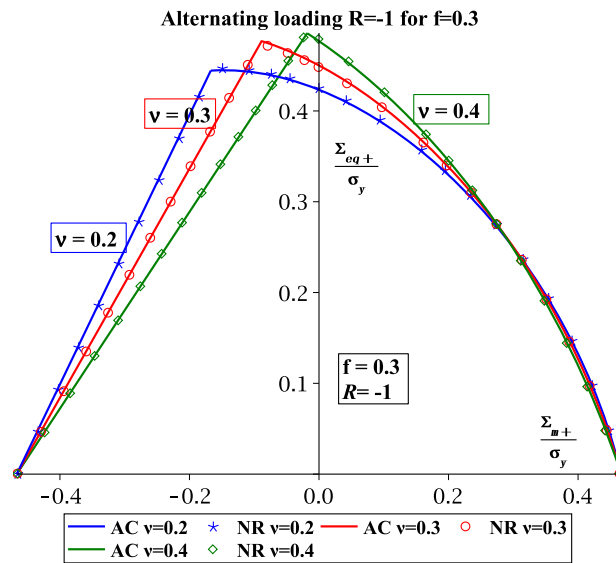


Figure 18: Comparison between the limit surfaces of the analytical criteria (AC) and numerical results (NR) for porosity $f = 0.3$ under alternating loadings $R = -1$ with respect to different values of Poisson's ratio of matrix: $\nu = 0.2$ (Blue), 0.3 (Red) and 0.4 (Green).

References

References

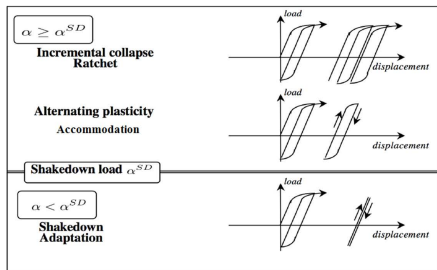
- 590 [1] Anoukou, K., Pastor, F., Dufrenoy, P., Kondo, D., 2016. Limit analysis and homogenization of porous materials with mohr-coulomb matrix. part i: Theoretical formulation. *Journal of the Mechanics and Physics of Solids* 91.
- [2] Balakrishnan, S., Veerappan, A., Shanmugam, S., 2019. Determination of plastic, shakedown and elastic limit loads of 90° pressurized pipe bends with shape imperfections. *International Journal of Pressure Vessels and Piping* 175, 103925.
- 595 [3] Benzerga, A. A., Besson, J., 2001. Plastic potentials for anisotropic porous solids. *European Journal of Mechanics-A/Solids* 20 (3), 397–434.
- [4] Bousshine, L., Chaaba, A., De Saxcé, G., 2003. A new approach to shakedown analysis for non-standard elastoplastic material by the bipotential. *International Journal of Plasticity* 19 (5), 583–598.
- 600 [5] Cao, Y., Shen, W., Shao, J.-F., Burlion, N., 2018. Influences of micro-pores and meso-pores on elastic and plastic properties of porous materials. *European Journal of Mechanics-A/Solids* 72, 407–423.
- [6] Cao, Y., Shen, W., Shao, J.-F., Wang, W., 2020. Numerical homogenization of elastic properties and plastic yield stress of rock-like materials with voids and inclusions at same scale. *European Journal of Mechanics-A/Solids* 81, 103958.
- 605 [7] Cazacu, O., Revil-Baudard, B., Lebensohn, R. A., Gă răjeu, M., 2013. On the combined effect of pressure and third invariant on yielding of porous solids with von mises matrix. *Journal of Applied Mechanics* 80 (6), 064501.
- [8] Cazacu, O., Stewart, J. B., 2009. Analytic plastic potential for porous aggregates with matrix exhibiting tension–compression asymmetry. *Journal of the Mechanics and Physics of Solids* 57 (2), 325–341.
- 610 [9] Cheng, L., de Saxcé, G., Kondo, D., 2014. A stress-based variational model for ductile porous materials. *International Journal of Plasticity* 55, 133–151.
- [10] Cheng, L., Guo, T., 2007. Void interaction and coalescence in polymeric materials. *International Journal of Solids and Structures* 44 (6), 1787–1808.
- [11] Cheng, L., Jia, Y., Oueslati, A., De Saxcé, G., Kondo, D., 2015. A bipotential-based limit analysis and homogenization of ductile porous materials with non-associated drucker-prager matrix. *Journal of the Mechanics and Physics of Solids* 77, 1–26.
- 615 [12] Cheng, L., Monchiet, V., Morin, L., De Saxcé, G., Kondo, D., 2015. An analytical lode angle dependent damage model for ductile porous materials. *Engineering Fracture Mechanics* 149, 119–133.
- [13] Dang-Van, K., 1973. Sur la résistance à la fatigue des métaux. Extrait de sciences et techniques de l’armement. *Mémorial de l’artillerie*. Troisième fascicule.
- 620 [14] Dang-Van, K., 1993. Macro-micro approach in high-cycle multiaxial fatigue. In: *Advances in multiaxial fatigue*. ASTM International.
- [15] De Saxcé, G., 1995. A variational deduction of the upper and lower bound shakedown theorems by markov and hill’s principles over a cycle. In: *Inelastic Behaviour of Structures under Variable Loads*. Springer, pp. 153–167.
- 625 [16] Druyanov, B., Roman, I., 1997. Concept of the limit yield condition in shakedown theory. *International journal of solids and structures* 34 (13), 1547–1556.
- [17] Feng, X.-Q., Liu, X.-S., 1996. On shakedown of three-dimensional elastoplastic strain-hardening structures. *International journal of plasticity* 12 (10), 1241–1256.
- 630 [18] Gă răjeu, M., Suquet, P., 1997. Effective properties of porous ideally plastic or viscoplastic materials containing rigid particles. *Journal of the Mechanics and Physics of Solids* 45 (6), 873–902.
- [19] Giugliano, D., Cho, N.-K., Chen, H., Gentile, L., 2019. Cyclic plasticity and creep-cyclic plasticity behaviours of the sic/ti-6242 particulate reinforced titanium matrix composites under thermo-mechanical loadings. *Composite Structures* 218, 204–216.
- 635 [20] Gokhfeld, D., 1956. Some problems of plastic shakedown of plates and shells (in russian). In: *Proc. 6th Soviet Conf. Plates and Shells (Bakou)*, Izd. Nauka, Moscou. pp. 284–291.

- [21] Gologanu, M., Leblond, J. B., Devaux, J., 1993. Approximate models for ductile metals containing non-spherical voids—case of axisymmetric prolate ellipsoidal cavities. *Journal of the Mechanics and Physics of Solids* 41 (11), 1723–1754.
- 640 [22] Gologanu, M., Leblond, J.-B., Perrin, G., Devaux, J., 1997. Recent extensions of gurson’s model for porous ductile metals. In: *Continuum micromechanics*. Springer, pp. 61–130.
- [23] Green, R., 1972. A plasticity theory for porous solids. *International Journal of Mechanical Sciences* 14 (4), 215–224.
- [24] Guo, T., Faleskog, J., Shih, C., 2008. Continuum modeling of a porous solid with pressure-sensitive dilatant matrix. *Journal of the Mechanics and Physics of Solids* 56 (6), 2188–2212.
- 645 [25] Gurson, A. L., et al., 1977. Continuum theory of ductile rupture by void nucleation and growth: Part i: Yield criteria and flow rules for porous ductile media. *Journal of engineering materials and technology* 99 (1), 2–15.
- [26] Halphen, B., 1980. Periodic solutions in plasticity and viscoplasticity. In: *Variational Methods in the Mechanics of Solids*. Elsevier, pp. 273–277.
- 650 [27] Heitzer, M., Staat, M., Reiners, H., Schubert, F., 2003. Shakedown and ratchetting under tension–torsion loadings: analysis and experiments. *Nuclear engineering and design* 225 (1), 11–26.
- [28] HILL, R., 1948. A variational principle of maximum plastic work in classical plasticity. *Quarterly Journal of Mechanics & Applied Mathematics* 1 (1), 18–28.
- 655 [29] Huang, S., Hui, H., Chen, Z., 2020. Numerical limit and shakedown analysis method for kinematic hardening structure made of arbitrary inhomogeneous material. *Composite Structures* 234, 111641.
- [30] Huang, S., Xu, Y., Chen, G., Zhang, L., Bezold, A., Qin, F., 2019. A numerical shakedown analysis method for strength evaluation coupling with kinematical hardening based on two surface model. *Engineering Failure Analysis* 103, 275–285.
- 660 [31] Jeong, H. Y., 2002. A new yield function and a hydrostatic stress-controlled void nucleation model for porous solids with pressure-sensitive matrices. *International Journal of Solids and Structures* 39 (5), 1385–1403.
- [32] Keralavarma, S., Benzerga, A., 2010. A constitutive model for plastically anisotropic solids with non-spherical voids. *Journal of the Mechanics and Physics of Solids* 58 (6), 874–901.
- 665 [33] Kobayashi, H., Kusumoto, T., Nakazawa, H., 1992. The cyclic j-r curve and upper-limit characteristic of fatigue-crack growth in 2-1/2 cr-mo steel. *International Journal of Pressure Vessels and Piping* 52 (52), 337–356.
- [34] Koiter, W. T., 1960. General theorems for elastic plastic solids. *Progress of solid mechanics*, 167–221.
- [35] König, J. A., 2012. *Shakedown of elastic-plastic structures*. Elsevier.
- 670 [36] Lacroix, R., Leblond, J.-B., Perrin, G., 2016. Numerical study and theoretical modelling of void growth in porous ductile materials subjected to cyclic loadings. *European Journal of Mechanics-A/Solids* 55, 100–109.
- [37] Madou, K., Leblond, J.-B., 2012. A gurson-type criterion for porous ductile solids containing arbitrary ellipsoidal voids—i: Limit-analysis of some representative cell. *Journal of the Mechanics and Physics of Solids* 60 (5), 1020–1036.
- 675 [38] Maier, G., Carvelli, V., Cocchetti, G., 2000. On direct methods for shakedown and limit analysis. *European Journal of Mechanics - A/Solids* 19 (Special Issue), S79–S100.
- [39] Manson, S. S., 1953. Behavior of materials under conditions of thermal stress. Vol. 2933. National Advisory Committee for Aeronautics.
- 680 [40] Markov, A., 1948. On variational principles in the theory of plasticity. Division of Applied Mathematics, Brown University.
- [41] Mbiakop, A., Constantinescu, A., Danas, K., 2015. On void shape effects of periodic elasto-plastic materials subjected to cyclic loading. *European Journal of Mechanics-A/Solids* 49, 481–499.
- [42] Melan, E., 1936. Theory statisch unbestimmter systeme aus ideal plastischen baustoff. *Sitz Ber Akad. Wiss*, 145–195.
- 685 [43] Monchiet, V., Cazacu, O., Charkaluk, E., Kondo, D., 2008. Macroscopic yield criteria for plastic anisotropic materials containing spheroidal voids. *International Journal of Plasticity* 24 (7), 1158–1189.

- [44] Monchiet, V., Charkaluk, E., Kondo, D., 2007. An improvement of gurson-type models of porous materials by using eshelby-like trial velocity fields. *Comptes Rendus Mecanique* 335 (1), 32–41.
- 690 [45] Monchiet, V., Kondo, D., 2013. Combined voids size and shape effects on the macroscopic criterion of ductile nanoporous materials. *International Journal of Plasticity* 43, 20–41.
- [46] Pastor, F., Kondo, D., Pastor, J., 2013. Limit analysis and computational modeling of the hollow sphere model with a mises–schleicher matrix. *International Journal of Engineering Science* 66, 60–73.
- [47] Peng, H., Liu, Y., Chen, H., Shen, J., 2018. Shakedown analysis of engineering structures under multiple
695 variable mechanical and thermal loads using the stress compensation method. *International Journal of Mechanical Sciences* 140, 361–375.
- [48] Qian, J., Dai, Y., Huang, M., 2020. Dynamic shakedown analysis of two-layered pavement under rolling-sliding contact. *Soil Dynamics and Earthquake Engineering* 129, 105958.
- [49] Save, M. A., Massonnet, C. E., De Saxcé, G., 1997. Plastic limit analysis of plates, shells and disks. Vol. 43. Elsevier.
- 700 [50] Sawczuk, A., 1969. Evaluation of upper bounds to shakedown loads for shells. *Journal of the Mechanics and Physics of Solids* 17 (4), 291–301.
- [51] Shen, W., Cao, Y., Shao, J.-F., Liu, Z., 2020. Prediction of plastic yield surface for porous materials by a machine learning approach. *Materials Today Communications*, 101477.
- 705 [52] Shen, W., Shao, J.-F., Kondo, D., Gatmiri, B., 2012. A micro–macro model for clayey rocks with a plastic compressible porous matrix. *International journal of plasticity* 36, 64–85.
- [53] Shen, W. Q., Oueslati, A., De Saxcé, G., 2015. Macroscopic criterion for ductile porous materials based on a statically admissible microscopic stress field. *International Journal of Plasticity* 70, 60–76.
- [54] Smith, M., 2009. Abaqus/standard user’s manual, version 6.9. Providence, RI: Simulia.
- 710 [55] Soutas-Little, R. W., 1999. Elasticity. Courier Corporation.
- [56] Sun, Y., Duo, W., 1989. A lower bound approach to the yield loci of porous materials. *Acta Mechanica Sinica* 5 (3), 237–243.
- [57] Sun, Y., Wang, D., 1989. Analysis of shear localization in porous materials based on a lower bound approach. *International Journal of Fracture* 71 (1), 71–83.
- 715 [58] Symonds, P. S., 1951. Shakedown in continuous media. *Journal of Applied Mechanics Transactions of the Asme* 18 (1), 85–89.
- [59] Tvergaard, V., 1981. Influence of voids on shear band instabilities under plane strain conditions. *International Journal of fracture* 17 (4), 389–407.
- [60] Tvergaard, V., Needleman, A., 1984. Analysis of the cup-cone fracture in a round tensile bar. *Acta metallurgica* 32 (1), 157–169.
- 720 [61] Varandas, J., Paixão, A., Fortunato, E., Coelho, B. Z., Hölscher, P., 2020. Long-term deformation of railway tracks considering train-track interaction and non-linear resilient behaviour of aggregates—a 3d fem implementation. *Computers and Geotechnics* 126, 103712.
- [62] Weichert, D., Maier, G., 2014. Inelastic behaviour of structures under variable repeated loads: direct analysis methods. Vol. 432. Springer.
- 725 [63] Weichert, D., Ponter, A., 2014. A historical view on shakedown theory. In: *The History of Theoretical, Material and Computational Mechanics-Mathematics Meets Mechanics and Engineering*. Springer, pp. 169–193.
- [64] Zhang, B., Wang, R., Hu, D., Jiang, K., Hao, X., Mao, J., Jing, F., 2020. Constitutive modelling of ratcheting behaviour for nickel-based single crystal superalloy under thermomechanical fatigue loading considering microstructure evolution. *International Journal of Fatigue* 139, 105786.
- 730 [65] Zhang, J., Oueslati, A., Shen, W., De Saxcé, G., Nguyen, A., Zhu, Q., Shao, J.-F., 2020. Shakedown analysis of a hollow sphere by interior-point method with non-linear optimization. *International Journal of Mechanical Sciences* 175, 105515.
- 735 [66] Zhang, J., Oueslati, A., Shen, W. Q., De Saxcé, G., 2019. Shakedown of porous material with drucker-prager dilatant matrix under general cyclic loadings. *Composite Structures* 220, 566–579.
- [67] Zhang, J., Shen, W., Oueslati, A., De Saxcé, G., 2017. A macroscopic criterion of shakedown limit for ductile porous materials subjected to general cyclic loadings. *Mechanics of Materials* 115, 76–87.

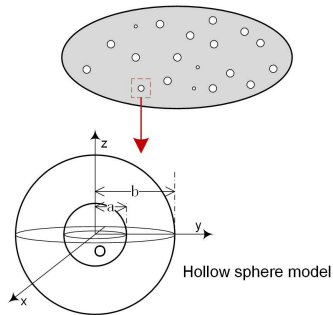
- 740 [68] Zhang, J., Shen, W., Oueslati, A., De Saxcé, G., 2017. Shakedown of porous materials. *International Journal of Plasticity* 95, 123–141.
- [69] Zhang, J., Shen, W., Zhu, Q., Shao, J.-F., 2020. A homogenized macroscopic criterion for shakedown analysis of ductile porous media with kinematical hardening matrix. *European Journal of Mechanics-A/Solids*, 104015.
- 745 [70] Zhang, Z., Cinoglu, I. S., Charbal, A., Vermaak, N., Lou, L., Zhang, J., 2020. Cyclic inelastic behavior and shakedown response of a 2nd generation nickel-base single crystal superalloy under tension-torsion loadings: Experiments and simulations. *European Journal of Mechanics-A/Solids* 80, 103895.
- [71] Zheng, X., Chen, H., Ma, Z., 2018. Shakedown boundaries of multilayered thermal barrier systems considering interface imperfections. *International Journal of Mechanical Sciences* 144, 33–40.
- 750 [72] Zhuang, Y., Wang, K.-Y., Li, H.-X., Wang, M., Chen, L., 2019. Application of three-dimensional shakedown solutions in railway structure under multiple hertz loads. *Soil Dynamics and Earthquake Engineering* 117, 328–338.
- [73] Ziya-Shamami, M., Babaei, H., Mostofi, T. M., Khodarahmi, H., 2020. Structural response of monolithic and multi-layered circular metallic plates under repeated uniformly distributed impulsive loading: An experimental study. *Thin-Walled Structures* 157, 107024.

Asymptotic responses under cyclic loadings



- Incremental collapse
- Alternating plasticity
- shakedown

Micromechanics-based model for porous materials



Variational-based principle

$$\mathcal{F} = \int_{\Omega} \int D(\dot{\epsilon}^p) dt dV - \int_{\Omega} \int \sigma^E : \dot{\epsilon}^p dt dV$$

Macroscopic fatigue criteria and numerical verifications

